Prebiotic photoredox synthesis from carbon dioxide and sulfite

Ziwei Liu[1], Long-Fei Wu[1], Corinna L. Kufner[2], Dimitar D. Sasselov[2], Woodward W. Fischer[3] and John D. Sutherland[1]*

[1]MRC Laboratory of Molecular Biology, Francis Crick Avenue, Cambridge Biomedical Campus, Cambridge, CB2 0QH, UK. [2]Harvard-Smithsonian Center for Astrophysics, Cambridge, Massachusetts, MA 02138, USA. [3]Division of Geological and Planetary Sciences, California Institute of Technology, Pasadena, CA 91125, USA.

*Correspondence to: johns@mrc-lmb.cam.ac.uk

Carbon dioxide (CO_2) is the major carbonaceous component of many planetary atmospheres including the Earth throughout its history, and prebiological chemistry that reduces this C_1 feedstock to organics has accordingly been sought. Carbon fixation chemistry utilizing hydrogen as stoichiometric reductant tends to require high pressures and temperatures, and yields of products of potential use to nascent biology are low[1]. Here we demonstrate efficient ultraviolet (UV) photoredox chemistry between CO_2 and sulfite (SO_3^{2-}) that generates organics and sulfate (SO_4^{2-}). The chemistry is initiated by electron photodetachment from SO_3^{2-} giving sulfite radicals and hydrated electrons, which reduce CO_2 to its radical anion. By subjecting individual products and putative intermediates to the reaction conditions and analyzing the resultant mixtures, a network of ensuing reactions that can rationalize the products was revealed. In this way it was further discovered that citrate, malate, succinate, and tartrate can be generated by irradiation of glycolate in the presence of SO_3^{2-}. The simplicity of this carboxysulfitic chemistry and the widespread occurrence and abundance of its feedstocks suggest that it could have readily taken place on the early Earth as well as on the surfaces of many rocky planets. The environmental availability of the carboxylate products on Earth could have driven the development of central carbon metabolism before the advent of biological CO_2 fixation.

Introduction

Many CO_2 reduction reactions have been discussed in the context of prebiotic chemistry, but all are problematic in that they require very special conditions and/or materials that are simply rare on planetary surfaces. For example, reduction by hydrogenation of bicarbonate (HCO_3^-) over a Ni-Fe alloy under hydrothermal conditions[2] requires high temperatures and pressures, and predominantly generates the C_1 product methane, a poor feedstock for elaboration into (proto)biomolecules. By separating H_2 and CO_2 with a thin Fe(Ni)S precipitate barrier across which there is a large pH difference, milder conditions enable reduction, but the product formate (HCO_2^-) is only produced in trace amounts[3]. Reduction of CO_2 using metallic Fe powder in water generates acetate, methanol, formate and pyruvate – the latter only transiently – but the widespread occurrence of Fe powder on rocky planets such as early Earth or Mars is unlikely[4]. Finally, UV photoreduction of CO_2 on colloidal ZnS semiconductor particles using hydrogen sulfide/hydrosulfide (H_2S/HS^-) as a hole scavenger gives formate, acetate and propionate in low yield[5], but these conditions are not likely to be common in a planetary context.

We previously demonstrated that hydrogen cyanide (HCN) can be reductively homologated using hydrated electrons (and/or hydrogen atoms derived therefrom by protonation) generated by UV irradiation of sulfidic anions in a process we termed cyanosulfidic chemistry[6]. For this chemistry, we originally used H_2S/HS^- as stoichiometric reductant, but switched to using bisulfite[7] (HSO_3^-, pK_a ~7.2)/SO_3^{2-} because sulfur dioxide (SO_2) and H_2S are outgassed in a ~10:1 or greater ratio on Earth[8-9], and there is substantial evidence from the geological records of both Earth and Mars via the anomalous mass fractionation of sulfur isotopes that these sulfur species were important constituents of the early sulfur cycle[10-11]. The Henry's law constant for SO_2 is greater than that of H_2S and the first pK_a of hydrated SO_2 (~1.9) is far lower than that of H_2S (~7.1)[12], so dissolution and hydration of SO_2 in surficial water followed by dissociation would therefore have been greater than dissolution and dissociation of H_2S on early Earth and Mars. Based on reports that hydrated electrons generated by UV illuminating diamond surfaces reduce CO_2 to carbon monoxide (CO) in acidic aqueous solution[13], and the aforementioned semiconductor UV photoreduction of CO_2, we now wondered if HSO_3^-/SO_3^{2-} could serve as the source of hydrated electrons for CO_2 reduction by UV photodetachment[14]. Given that alkaline lakes can simultaneously absorb atmospheric CO_2 and SO_2 to give HCO_3^- and SO_3^{2-} and a growing body of evidence that suggests that such lakes could have concentrated other

prebiotically important species on early Earth and maybe Mars[15-16], we started to explore reduction chemistry at mildly alkaline pH.

Results and discussion

We subjected an aqueous solution of the sodium salts of HCO_3^- **1** (50 mM) and SO_3^{2-} (100 mM) at pH = 9 to UV irradiation from Hg-lamps with principal emission at 254 nm in a standard laboratory UV photoreactor and analyzed the resultant mixture by ^{1}H-NMR spectroscopy, integrating signals relative to those of a subsequently added standard to quantitate products. After 4 hours irradiation, formate **2** (18 mM), hydroxymethanesulfonate **3** (200 μM), methanol **4** (200 μM), glycolate **5** (200 μM), acetate **6** (50 μM), tartronate **7** (600 μM), and malonate **8** (300 μM) had been produced alongside both *rac*- and *meso*-tartrate **9a** (30 μM) and **9b** (30 μM) (structures of products shown in Fig. 1, Fig. S1). Sulfate was detected as a photoredox co-product[14] by precipitation of barium sulfate upon addition of barium chloride under conditions where barium sulfite is soluble[17]. The bicarbonate-sulfite irradiation experiment was repeated using ^{13}C-labelled HCO_3^- **1** to confirm that all the products were generated from the photoreduction of CO_2, and all product assignments were confirmed by spiking with authentic standards (Fig. S1, Fig. S2). Surprisingly, we were able to detect elemental hydrogen (H_2) by ^{1}H-NMR spectroscopy (δ = 4.5 ppm) if it was generated *in situ* by performing the irradiation experiment in a quartz NMR tube. This peak decreased/disappeared simply by shaking the NMR tube presumably because this accelerated degassing. The signal assignment for H_2 was confirmed by running an NMR spectrum of the products of mixing zinc with hydrochloric acid solution in an NMR tube (Fig. S3). Taken together, these results show that HCO_3^- **1** is reductively converted to C_2, C_3 and (traces of) C_4 compounds as well as being reduced to other C_1 compounds in a process that also generates H_2 and SO_4^{2-}. If the initial concentration of HCO_3^- **1** was reduced to 5 mM and the concentration of SO_3^{2-} reduced to 10 mM, formate **2** (30 μM), glycolate **5** (20 μM), acetate **6** (10 μM), tartronate **7** (120 μM), and malonate **8** (30 μM) were observed by ^{1}H-NMR spectroscopy after 4 hours irradiation. The combined yield of organics in these experiments exceeded 10% demonstrating the remarkably high efficiency of this chemistry compared to other potentially prebiotic CO_2 fixation processes (Fig. S4, Extended Data Table 1). In addition to the protiated products observed by ^{1}H-NMR spectroscopy, oxalate **10** was observed by ^{13}C-NMR spectroscopy in yields as high as 11% (Fig. S5). At higher concentrations

of reactants, the yield of C_1 products, especially formate **2**, went up relative to the yield of $C_{>1}$ products and after prolonged irradiation, a new C_3 product, β-hydroxypropionate **11** was identified (Fig. S6).

We next investigated the photoreaction of the various products and some putative intermediates in the presence of SO_3^{2-} with a view to gaining information concerning the mechanism of the fixation chemistry. The results – summarized in Extended Data Table 2 (Fig. S7 – S18) – can be rationalized by a reaction network based on photoredox radical chemistry (Fig. 1). Photodetachment of an electron from SO_3^{2-} gives a hydrated electron and a sulfite radical ($\cdot SO_3^-$)[14]. At pH 9, both loss of hydroxide from HCO_3^- **1** and loss of water from its conjugate acid, H_2CO_3, furnish CO_2. The latter process is efficiently catalyzed by sulfite[18], so it is unlikely that the otherwise slow kinetics of equilibration limit the photoredox chemistry. Although the equilibrium concentration of CO_2 is very low in a solution containing HCO_3^- **1** at pH = 9 relative to the concentration of **1**, the rate constant for reaction of CO_2 with hydrated electrons to give the carboxyl radical **12** is extremely high[19] and greatly exceeds the rate constant at atmospheric pressure for protonation of hydrated electrons by **1** giving hydrogen atoms[20]. The carboxyl radical **12** can either be reduced by hydrogen atom transfer (HAT) from HSO_3^-, which has a ~1% abundance relative to SO_3^{2-} at pH = 9, to give formate **2**, or undergo dimerization to give oxalate **10**, both directly and indirectly[21]. Focussing on the chemistry of formate **2** first, one electron reduction, though relatively slow[22], gives the radical anion **13** and thence, through acid-base and hydration equilibria, the radicals **14** and **15** (although the latter is unfavoured relative to **13** and **14**). The radicals **13** and **14** have two main fates; reduction by HAT from HSO_3^-, or recombination with the carboxyl radical **12**. Coupled with acid-base and hydration equilibria, the first process (shown only for **13**), generates formaldehyde **16** and its hydrate **17** and the second (shown only for **14**) generates glyoxylate **18** via its hydrate **19**. Formaldehyde **16**, in equilibrium with the bisulfite adduct **3**, can be reduced to the radical **20** which gives methanol **4** by HAT and glycolate **5** by recombination with the carboxyl radical **12**[23]. Another major reaction of formate **2** is oxidation back to carboxyl radicals **12** by reaction with sulfite radicals. This is inferred from the observation that irradiation of formate **2** and SO_3^{2-} gives significant amounts of what appear to be products deriving from oxalate **10** in addition to C_1 products (Extended Data Table 2).

The other initial product of the carboxyl radical **12** – its dimer oxalate **10** – can be reduced by addition of a hydrated electron to give the radical anion **21**[24]. This reduction is much faster than the corresponding reduction of formate **2**. The radical anion **21** can undergo HAT leading to glyoxylate hydrate **19**, or recombination with another carboxyl radical **12** to give mesoxalate hydrate **22**, which equilibrates with mesoxalate **23**[25]. Reduction of mesoxalate **23** by addition of a hydrated electron, or electron transfer from a carboxyl radical **12**, followed by HAT gives tartronate **7** and deoxygenation of the latter followed by HAT gives malonate **8**. In the same multistep way that formate **2** can be reduced to methanol **4**, reduction of one of the carboxylate groups of malonate **8** leads to β-hydroxypropionate **11**. Reduction of glyoxylate **18** (in equilibrium with the hydrate **19** and a bisulfite adduct, not shown)[26] and protonation of the initially formed radical anion[27] leads to the key hydroxy-carboxymethyl radical **24** (pK_a~8.8)[28] which can recombine with the carboxyl radical **12** to give tartronate **7**, dimerize to give the tartrates **9**, or undergo HAT to give glycolate **5**. Deoxygenation of glycolate **5** gives the carboxymethyl radical **25**, which by recombination with the carboxyl radical **12** can give malonate **8**[29] and by HAT, acetate **6**.

Finally, we identified a number of photochemical steps other than the photodetachment of electrons from SO_3^{2-}, which initiates the reaction network. Norrish type I reactions of glyoxylate **18** and mesoxalate **23** generate radicals **12**, **15** and **26** (similar photocleavage of malonsemialdehyde **27**, en route to β-hydroxypropionate **11**, would generate radicals **15** and **25**) and photodetachment of an electron from oxalate **10**[30-31] gives radical **28** which is thought to decarboxylate to the carboxyl radical **12**. These additional photochemical steps set up futile cycles in the network, but also forge links from the $C_{>1}$ parts of the network to the C_1 part (Fig. S19 – S23).

Based on the foregoing analysis, we thought that it might be possible to increase the amount of the $C_{>1}$ products by adding sulfite portionwise – this would ensure that at any one time, the concentration of HSO_3^- would be low, so reaction flux through oxalate **10** would be favoured, but overall, there would be more reduction capacity. In accordance with expectation, at the end of this experiment, the combined yield of $C_{>1}$ products (>25%) greatly exceeded C_1 products (<1%) and the combined yield of malonate **8** (16.2%) and acetate **6** (1.0%) was greater than twice that of tartronate **7** (6.6%) and glycolate **5** (0.8%). Unexpectedly, a new product,

sulfoacetate **29** (0.8%) was formed in low yield presumably through recombination of carboxymethyl radicals **25** with sulfite radicals. (Fig. S24, Extended Data Table 1). The general features of the time course of the CO_2 reduction network were also revealed by this experiment. After 1 hour, formate **2** was the major product accompanied by traces of glycolate **5** and tartronate **7**. After 2 hours, the amount of formate **2** had decreased and glycolate **5** and tartronate **7** were now the major products along with smaller amounts of acetate **6** and malonate **8**. After further irradiation, the levels of formate **2**, glycolate **5** and tartronate **7** stayed at about the same level and malonate **8** became the major product with minor amounts of acetate **6** and methanol **4**. This time course behaviour can be understood from the reaction network (Fig. 1). At the outset of the experiment, the only carbonaceous species for the hydrated electrons to reduce is CO_2. Carboxyl radicals **12** thereby produced apparently undergo HAT from HSO_3^- faster than they dimerise, and so formate **2** increases. However, the conversion of carboxyl radicals **12** to **2** is reversible, and so after some time a sufficient amount of oxalate **10** is produced for it to be reduced by the hydrated electrons as well. The reduction of oxalate **10** is much faster than the reduction of formate **2** (investigated by ultrafast pump-probe spectroscopy and further discussed in the SI), so **2** is consumed at the expense of making reduction products of **10**. The appearance of the radical anion **21** opens up a new path for consumption of carboxyl radicals **12**, including recombination to give mesoxalate hydrate **22** that is rapidly converted to tartronate **7** and a new path for the consumption of HSO_3^-, namely HAT to **21** giving glyoxylate **18** and thence, through rapid further reduction, glycolate **5**. The opening of these new reaction paths reduces the level of formate **2** to a steady state where its consumption is balanced by continuous production from CO_2 via carboxyl radicals **12**. Eventually, the deoxygenation of tartronate **7** coupled to the slow reduction of malonate **8** means that the latter becomes the predominant product. At higher initial concentrations of sulfite, the early formate **2** pulse lasts longer and produces higher early amounts of **2**, but eventually the paths to $C_{>1}$ products start to operate and levels of formate **2** drop. Even if formate **2** is reduced, the reversibility of the downstream steps to C_1 products and other paths from the C_1 part of the network to the $C_{>1}$ part mean that products more complex than **2** eventually accumulate.

As we investigated the photoreactions of the products and putative intermediates of the CO_2 reduction network with SO_3^{2-}, the photoredox chemistry of one product – glycolate **5** – stood out. Acetate **6** (16.2 mM), malonate **8** (0.1 mM), sulfoacetate **29** (7.8 mM), citrate **30** (0.2 mM),

rac-tartrate **9a** (1.5 mM), *meso*-tartrate **9b** (1.0 mM), malate **31** (2.9 mM), succinate **32** (1.1 mM) and hydroxycitrate **33** (0.19 mM) along with C_1 products were detected by ^{1}H-NMR spectroscopy after 6 hours irradiation of glycolate **5** (50 mM) and SO_3^{2-} (100 mM) (Fig. S11). Particularly noteworthy is the fact that citrate **30**, malate **31** and succinate **32** are key constituents of the Krebs cycle – a major cycle of central carbon metabolism, the consequences of which are discussed below. Remarkably, when the concentration of glycolate **5** was reduced to 5 mM and the concentration of SO_3^{2-} reduced to 10 mM, after 2 hours irradiation, C_1 products were no longer detected but the higher products were still formed in a comparable overall yield albeit with a different relative abundance distribution (Fig. S12). The chemistry that generates acetate **6**, malonate **8** and the tartrates **9** is the same as some of that of the CO_2 fixation reaction network, but additional reactions now contribute to the detectable products (Fig. 2). Abstraction of a hydrogen atom from glycolate **5** by a sulfite radical generates the hydroxy-carboxymethyl radical **24** whilst redox compensatory reduction of **5** generates the carboxymethyl radical **25**. Dimerization of **24** produces the tartrates **9** whereas dimerization of **25** produces succinate **32** as well as acetate **6** and glycolate **5**[32]. Recombination of radicals **24** and **25** provides one route to malate **31**, a second would be from reduction of **9**. Similar reduction of malate **31** would give a second path to succinate **32**. Oxidation of the tartrates **9** and malate **31** to the corresponding hydroxyalkyl radicals **34** and **35** followed by recombination of these radicals with radicals **24** or **25** would give dihydroxycitrate **36**, hydroxycitrate **33** and citrate **30**. Reduction of **36** would constitute another reaction channel to hydroxycitrate **33** and further reduction of **33**, another channel to citrate **30**. In contrast to the reaction network starting from CO_2 where all products are reduced relative to the starting material, the network starting from glycolate **5** is more subtle and contains both carbon oxidations and reductions. Thus malate **31** and citrate **30** are at the same oxidation level as glycolate **5**, succinate **32** and acetate **6** are more reduced and the tartrates **9** and hydroxycitrate **33** are, on average, more oxidized.

We also evaluated the bicarbonate reduction chemistry using a less intense broadband UV source, StarLab[33] – an in-house constructed photoreactor designed to deliver UV radiation with a wavelength distribution representative of that from the Sun incident on the surface of early Earth, at a ~100 fold higher intensity than the Sun in a quiescent state and ~10 fold lower intensity than that during maximum flaring. After irradiation for 7 days in this apparatus, an aqueous solution of the sodium salts of HCO_3^- **1** (5 mM) and SO_3^{2-} (50 mM) at pH = 9 gave a mixture of protiated

products similar to that obtained upon higher intensity irradiation in the standard laboratory photoreactor (at 254 nm for shorter time intervals) plus ethanol **37**, confirming the utility of using 254 nm UV light to study this chemistry (Fig. S25, Extended Data Table. 1). Oxalate **10** was also detected in a similar experiment using ^{13}C-labelled bicarbonate (Fig. S26). Ethanol **37** could plausibly be obtained via dimerization of the hydroxymethyl radical **20** giving ethylene glycol **38**, dehydration of **38** through radical **39** and the enoloxy radical **40**[34] to acetaldehyde **41** and reduction (Fig. 1). Alternatively, acetate **6** could be reduced to acetaldehyde **41** and thence ethanol **37**.

We then investigated the carboxysulfitic photoredox chemistry of glycolate **5** in the StarLab photoreactor. After 8 hours irradiation of glycolate **5** (50 mM) and SO_3^{2-} (100 mM) with this less intense light source, acetate **6** (1.7 mM), sulfoacetate **29** (0.2 mM), *rac*-tartrate **9a** (0.4 mM), *meso*-tartrate **9b** (0.4 mM), malate **31** (0.2 mM), and succinate **32** (trace) along with C_1 products were detected by ^{1}H-NMR spectroscopy (Fig. S13, Extended Data Table. 2). Longer irradiation of more dilute samples of glycolate **5** (5 mM) and SO_3^{2-} (50 mM) in the StarLab photoreactor resulted in higher yields of the same species and additionally produced malonate **8** and hydroxypropionate **11** (Fig. S27).

Planetary relevance

An important aspect of this chemistry is that the conditions and materials necessary to foster carboxysulfitic carbon fixation (short wave UV light, CO_2 and SO_2 derived from volcanism, and bodies of standing and flowing water on the crust) are mild, widespread, and expected to be common on rocky planets. Notably, there is geological evidence from the rock records of Earth and Mars that these conditions were met early in their history. Oxygen isotope ratios from Hadean zircons[35-36] and sedimentological observations from the earliest sedimentary record[37] indicate abundant surface liquid water. Silicate weathering reactions occurred that sourced the alkalinity necessary to enable the dissociated hydrates, bicarbonate and sulfite, to partition from the atmosphere and accumulate in bodies of water in contact with the atmosphere[38]. Moreover, the anomalous fractionation of multiple sulfur isotopes in the early geological record[10] provides a direct measure of SO_2 photochemistry that establishes a valuable atmospheric correlate of the aqueous carbon fixation processes described herein. Finally, each of these observations for the early Earth that illustrates the plausibility of this chemistry occurring now has its complement in

the Mars geological record[11, 39-42]. Thus, the ingredients and basic conditions for carboxysulfitic chemistry to take place would have been present on both Earth and Mars.

The case for conditions conducive to cyanosulfidic chemistry being present on both young planets has also been made[43]. We note that for the full range of cyanosulfidic chemistry products to result, a scenario involving the mixing of bodies of water or flows (e.g. stream water) having subtly different reaction histories would probably be necessary. In locations where the basic conditions for cyanosulfidic chemistry were met, but the mixing of streams was absent or different, a limited set of products would have been generated and the first product of the restricted reaction network, glycolonitrile **42**, would probably have been the most widespread. In addition, glycolonitrile **42** could have resulted from reaction of HCN with formaldehyde **16** rained in after production in the upper atmosphere by photoreduction of CO_2[44]. Hydrolysis of the nitrile group of glycolonitrile **42**, however produced, generates glycolate **5** (Fig. 3), which could be partially converted by subsequent carboxysulfitic chemistry to the range of carboxylate products previously described. As the hydrolysis of glycolonitrile **42** generates ammonia in addition to glycolate **5**, we also carried out the irradiation of **5** and sulfite in the presence of ammonia. It transpired that ammonia did not affect the outcome of the photoredox chemistry – the same set of products was formed with or without ammonia (Fig. S28). In those locations where glycolonitrile **42** was not formed and hydrolyzed, carboxysulfitic chemistry from a CO_2 feedstock could still have been possible. In such places, which were probably more common than the locations in which cyanosulfidic chemistry took place, a more limited set of organics would have been produced. Depending on conditions, carboxylates such as formate **2**, oxalate **10** or acetate **6** and malonate **8** are likely to have been the major initial products. Decarboxylation of malonate **8** to acetate **6** occurs on a short geological timescale in solution (~10 years at neutral pH and at 25°C)[45] whereas oxalate **10** (in the absence of ferric ions and light)[46], like acetate **6** is long-term stable and so it seems likely that these latter two products would have become the most abundant $C_{>1}$ organics on early Earth had life not emerged – they might still be the most abundant organics on Mars if life did not emerge there.

Biochemical relevance

We suggest that life emerged in a location where the full scope of cyanosulfidic chemistry played out, but at a later date when conditions were more clement than those required to drive the reductive nitrile homologation chemistry. Use of the products of cyanosulfidic chemistry as

building blocks by nascent biology would eventually lead to their environmental depletion and biology would then be under evolutionary pressure to synthesize these building blocks from anything else that happened to be available and usable. Locations where cyanosulfidic chemistry was restricted to generating glycolonitrile **42**, or where **42** was generated from HCN and rained-in formaldehyde **16** would, following hydrolysis of **42** to glycolate **5** and subsequent carboxysulfitic chemistry, potentially have a menu of **5**, acetate **6**, malonate **8**, tartrate **9**, citrate **30**, malate **31** and succinate **32** present. Biology could either spread to encounter these materials in their place of synthesis, or fluvial advection could move them to the location of biology. It is fascinating that the majority of the carboxylate products deriving from glycolate **5** are key nodes of central carbon metabolism in extant biology and it seems likely that their synthesis by carboxysulfitic chemistry set the stage for the development of this metabolic network. At first glance, tartrate **9** seems to be somewhat an outlier, but its dehydration would lead through an enol to oxaloacetate[47] and its oxidation, to dihydroxyfumarate which spontaneously decarboxylates to give glycolaldehyde[48], a precursor of higher sugars.

With time, supply of most of the products of the carboxysulfitic chemistry of glycolate **5** would also dwindle and biology would have to evolve to make do with simpler, more abundant carbonaceous materials in the environment. The major long term stable products of the carboxysulfitic chemistry of CO_2 – formate **2**, acetate **6** and oxalate **10** – could then provision central carbon metabolism through development of a pyruvate-formate lyase activity and the glyoxylate shunt of the Krebs cycle via reduction of oxalate **10** to glyoxylate **18**. Finally, even oxalate **10** and acetate **6** would become depleted and biology would be under evolutionary pressure to use the only remaining abundant carbon source, namely CO_2.

According to this model based on the chemistry we have uncovered, the overall development of metabolism would be a gradual change from heterotrophy of photochemical products to autotrophy with biology being environmentally ‘weaned’ onto to ever simpler carbon sources (Fig. 3). By having a rich mix of amino acids, nucleotides and lipids from cyanosulfidic chemistry at the outset, life has the greatest chance to start and progress. By then accessing an array of carboxylates from the carboxysulfitic chemistry of glycolate **5**, central carbon metabolism could develop with late-synthetic-stage introduction of nitrogen, a hallmark of extant metabolism. More abundant, but less rich product mixtures derived through the carboxysulfitic

chemistry of CO_2 could then have sustained life until it acquired the ability to sustain itself from atmospherically sourced CO_2.

References

1. Muchowska, K. B., Varma, S. J. & Moran, J. Nonenzymatic metabolic reactions and life's origins. *Chem. Rev.* **120**, 7708–7744 (2020).
2. Horita, J. & Berndt, M. E. Abiogenic methane formation and isotopic fractionation under hydrothermal conditions. *Science* **285**, 1055–1057 (1999).
3. Hudson, R. et al. CO_2 reduction driven by a pH gradient. *Proc. Natl. Acad. Sci. USA* **117**, 22873–22879 (2020).
4. Varma, S. J., Muchowska, K. B., Chatelain, P. & Moran, J. Native iron reduces CO_2 to intermediates and end-products of the acetyl-CoA pathway. *Nature Ecol. Evol.* **2**, 1019–1024 (2018).
5. Zhang, X. V. et al. Photodriven reduction and oxidation reactions on colloidal semiconductor particles: Implications for prebiotic synthesis. *J. Photochem. Photobiol. Chem.* **185**, 301–311 (2007).
6. Patel, B. H., Percivalle, C., Ritson, D. J., Duffy, C. D. & Sutherland, J. D. Common origins of RNA, protein and lipid precursors in a cyanosulfidic protometabolism, *Nat. Chem.* **7**, 301–307 (2015).
7. Xu, J., et al. Photochemical reductive homologation of hydrogen cyanide using sulfite and ferrocyanide. *Chem. Commun.* **54**, 5566–5569 (2018).
8. Zahnle, K., Claire, M., & Catling, D. The loss of mass-independent fractionation in sulfur due to a Palaeo-proterozoic collapse of atmospheric methane. *Geobiology* **4**, 271–283 (2006).
9. Gerlach, T. M. Evaluation and restoration of the 1970 volcanic gas analyses from Mount Etna, Sicily. J. Volcanol. *Geotherm. Res.* **6**, 165–178 (1979).
10. Farquhar, J., Bao, H. & Thiemens, M. Atmospheric influence of Earth's earliest sulfur cycle. *Science* **289**, 756–758 (2000).

11. Farquhar, J., Savarino, J., Jackson, T. & Thiemens, M. H. Evidence of atmospheric sulphur in the martian regolith from sulphur isotopes in meteorites. *Nature* **404**, 50–52 (2000).

12. Ranjan, S., Todd, Z. R., Sutherland, J. D. & Sasselov, D. D. Sulfidic anion concentrations on early earth for surficial origins-of-life chemistry. *Astrobiology* **18**, 1023–1040 (2018).

13. Zhang, L., Zhu, D., Nathanson, G. M. & Hamers, R. J. Selective photoelectrochemical reduction of aqueous CO_2 to CO by solvated electrons. *Angew. Chem. Int. Ed.* **126**, 9904–9908 (2014).

14. Fischer, M. & Warneck, P. Photodecomposition and photooxidation of hydrogen sulfite in aqueous solution. *J. Phys. Chem.* **100**, 15111–15117 (1996).

15. Toner, J. D. & Catling, D. C. A carbonate-rich lake solution to the phosphate problem of the origin of life. *Proc. Natl. Acad. Sci. USA* **117** 883–888 (2020).

16. Toner, J. D. & Catling, D. C. Alkaline lake settings for concentrated prebiotic cyanide and the origin of life. *Geochim. Cosmochim. Acta* **260**, 124–132 (2019).

17. Malati, M. A. *Experimental inorganic/physical chemistry: an investigative, integrated approach to practical project work* (Woodhead Publishing Limited, 1999).

18. Roughton, F. J. W. & Booth, V. H. The catalytic effect of buffers on the reaction $CO_2 + H_2O = H_2CO_3$. *Biochem. J.*, **32**, 2049–2069 (1938).

19. Gordon, S., Hart, E. J., Matheson, M. S., Rabani, J. & Thomas, J. K. Reactions of the hydrated electron. *Discussions Faraday Soc.* **36**, 193–205 (1963).

20. Hentz, R. R., Farhataziz, Milner, D. J. & Burton, M., γ-Radiolysis of liquids at high pressures. III. Aqueous solutions of sodium bicarbonate. *J. Chem. Phys.* **47**, 374–377 (1967).

21. Flyunt, R, Schuchmann, M. N. & von Sonntag, C. A common carbanion intermediate in the recombination and proton-catalysed disproportionation of the carboxyl radical anion $CO_2^{\cdot-}$ in aqueous solution. *Chem. Eur. J.* **7**, 796–799 (2001).

22. Swallow, A. J. Recent results from pulse radiolysis. *Photochem. Photobiol.* **7**, 683–694 (1968).

359 23. Getoff, N., Gütlbauer, F. & Schenck, G. O. Strahlenchemische carboxylierung von
360 ameisensäure und methanol in wässriger lösung, *Int. J. Appl. Radiat. Isot.* **17**, 341–349
361 (1966).

362 24. Getoff, N, Schwörer, F., Markovic, V. M., Sehested, K. & Nielsen, S. O. Pulse radiolysis
363 of oxalic acid and oxalates. *J. Phys. Chem.* **75**, 749–755 (1971).

364 25. Doussin, J.-F. & Monod, A. Structure-activity relationship for the estimation of
365 OH-oxidation rate constants of carbonyl compounds in the aqueous phase. *Atmos. Chem.*
366 *Phys.* **13**, 11625–11641 (2013).

367 26. Olson, T. M. & Hoffmann, M. R. Formation kinetics, mechanism and thermodynamics of
368 glyoxylic acid–S(IV) adducts. *J. Phys. Chem.* **92**, 4246–4253 (1988).

369 27. Laroff, G. P. & Fessenden, R. W. ^{13}C Hyperfine interactions in radicals from some
370 carboxylic acids. *J. Chem. Phys.* **55**, 5000–5008 (1971).

371 28. Bell, J. A. Grunwald, E. & Hayon, E. Kinetics of deprotonation of organic free radicals in
372 water. Reaction of $HOC{\cdot}HCO_2^-$, $HOC{\cdot}HCONH_2$ and $HOC{\cdot}CH_3CONH_2$ with various
373 bases. *J. Am. Chem. Soc.* **97**, 2995–3000 (1975).

374 29. Getoff, N. CO_2 and CO utilization: radiation-induced carboxylation of aqueous
375 chloroacetic acid to malonic acid. *Radiat. Phys. Chem.* **67**, 617–621 (2003).

376 30. Arvis, M., Lustig H. & Hickel B. Étude par photolyse éclair de la photoionisation des
377 anions formiate, acetate et oxalate dans l'eau. *J. Photochem.* **13**, 223–232 (1980).

378 31. Huie R. E. & Clifton, C. L. Kinetics of the reaction of the sulfate radical with the oxalate
379 anion. *Int. J. Chem. Kinetics* **28**, 195–199 (1996).

380 32. Wang, W.-F., Schuchmann, M. N., Schuchmann, H.-P. & von Sonntag, C. The
381 importance of mesomerism in the termination of α-carboxymethyl radicals from aqueous
382 malonic and acetic acids. *Chem. Eur. J.* **7**, 791–795 (2001).

383 33. Rimmer, P. et al. Is ultraviolet light prebiotic? *Astrobiology* under review.

384 34. Gilbert, B. C., Larkin, J. P. & Norman, R. O. C. Electron spin resonance studies. Part
385 XXXIII. Evidence for heterolytic and homolytic transformations of radicals from
386 1,2-diols and related compounds. *J. Chem. Soc., Perkin Trans. 2* 794−802 (1972).

35. Wilde, S., Valley, J., Peck, W. & Graham, C. M. Evidence from detrital zircons for the existence of continental crust and oceans on the Earth 4.4 Gyr ago. *Nature* **409,** 175–178 (2001).

36. Valley, J. W. et al. 4.4 billion years of crustal maturation: oxygen isotope ratios of magmatic zircon. *Contrib. Mineral. Petrol.* **150**, 561–580 (2005).

37. Rosing, M. T. ^{13}C-Depleted carbon microparticles in >3700-Ma sea-floor sedimentary rocks from west Greenland. *Science* **283**, 674–676 (1999).

38. Kasting, J. F. The Goldilocks planet? How silicate weathering maintains Earth "just right". *Elements: An International Magazine of Mineralogy, Geochemistry, and Petrology* **15**, 235–240 (2019).

39. Grotzinger, J. P. et al. Deposition, exhumation, and paleoclimate of an ancient lake deposit, Gale crater, Mars. *Science* **350**, doi: 10.1126/science.aac7575. (2015).

40. DiBiase, R. A., Limaye, A. B., Scheingross, J. S., Fischer, W. W. & Lamb, M. P., Deltaic deposits at Aeolis Dorsa: Sedimentary evidence for a standing body of water on the northern plains of Mars. *J. Geophys. Res. Planets* **118**, 1285–1302 (2013).

41. Hurowitz, J. A. et al. Redox stratification of an ancient lake in Gale Crater, Mars. *Science* **356**, doi:10.1126/science.aah6849 (2017).

42. Milliken, R. E., Fischer, W. W. & Hurowitz, J. A. Missing salts on early Mars. *Geophys. Res. Letts.* **36**, doi:10.1029/2009GL038558 (2009).

43. Sasselov, D. D., Grotzinger, J. P. & Sutherland, J. D. The origin of life as a planetary phenomenon. *Sci. Adv.* **6**, doi:10.1126/sciadv.aax3419 (2020).

44. Cleaves II, H. J. The prebiotic geochemistry of formaldehyde. *Precambrian Res.* **164**, 111–118 (2008).

45. Wolfenden, R., Lewis, Jr., C. A. & Yuan Y. Kinetic challenges facing oxalate, malonate, acetoacetate and oxaloacetate decarboxylases. *J. Am. Chem. Soc.* **133**, 5683–5685 (2011).

46. Goldstein, S. & Rabani, J. The ferrioxalate and iodide–iodate actinometers in the UV region. *J. Photochem. Photobiol. A* **193**, 50–55 (2008).

47. Yew, W. S. et al. Evolution of enzymatic activities in the enolase superfamily: D-tartrate dehydratase from *Bradyrhizobium japonicum*. *Biochemistry* **45**, 14598–14608 (2006).

48. Sagi, V. N., Punna, V., Hu, F., Meher, G. & Krishnamurthy, R. Exploratory experiments on the chemistry of the "glyoxylate scenario": formation of ketosugars from dihydroxyfumarate. *J. Am. Chem. Soc.* **134**, 3577–3589 (2012).

Acknowledgements The authors thank J.D.S., D.D.S. and W.W.F. group members for helpful discussions. This research was supported by the Medical Research Council (MC_UP_A024_1009 to J.D.S.), the Simons Foundation (290362 to J.D.S. and 290360 to D.D.S.). C.L.K. and D.D.S. thank Wolfgang Zinth, Pablo Dominguez, Daniel Yahalomi, Gabriella Lozano for helpful discussions and experimental assistance, and acknowledge the Harvard Origins of Life Initiative.

Author contributions Z.L. discovered this carboxysulfitic chemistry and explored its scope under the supervision of J.D.S. and with the assistance of L.-F.W., C.L.K. performed the pump-probe experiments under the supervision of D.D.S., W.W.F. evaluated the geochemical relevance of the chemistry. All authors co-wrote the manuscript.

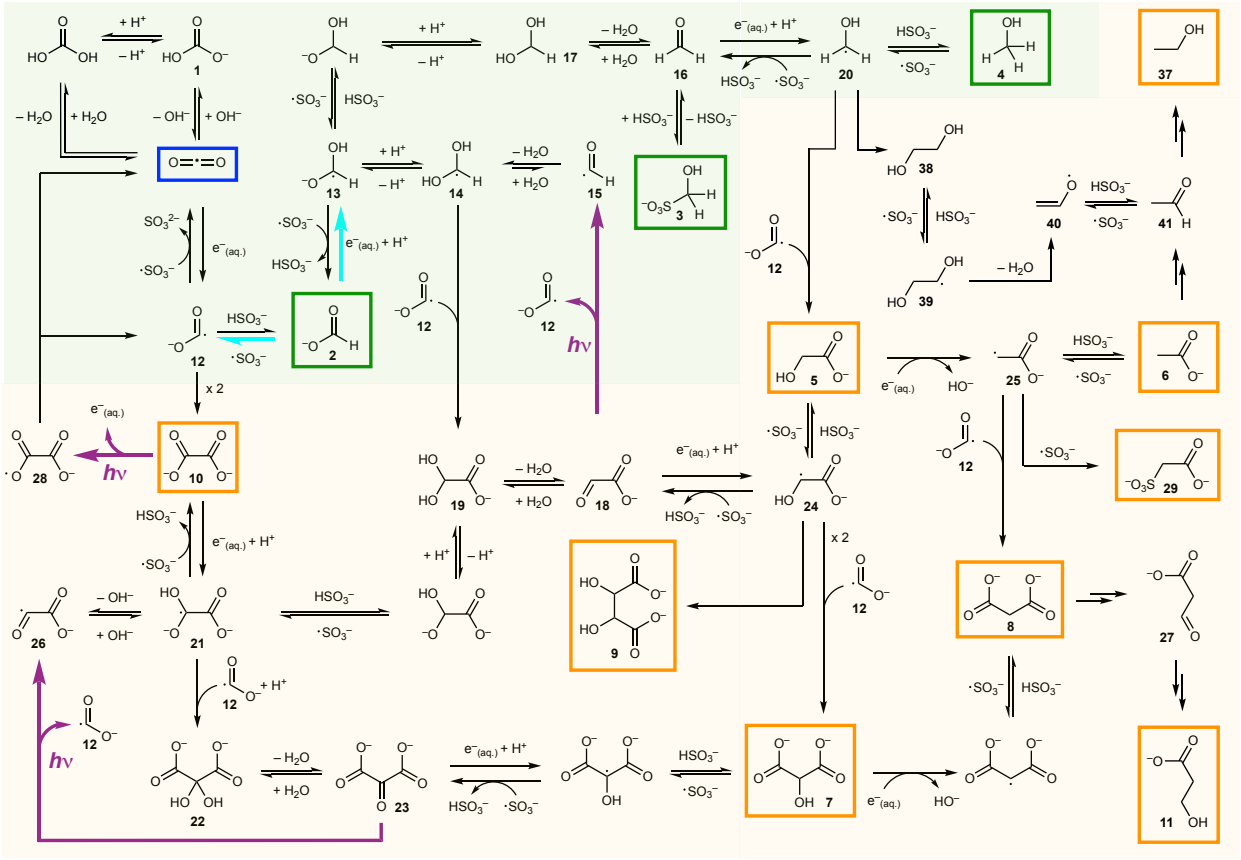

Fig. 1| Carboxysulfitic photoredox reaction network starting from bicarbonate (HCO_3^-) 1. Starting in the top left, the reaction network starts with the addition of hydrated electrons (produced by photodetachment from sulfite) to CO_2 (blue box) to give the carboxyl radical **12** after which point the network splits. Sequential reduction of the carboxyl radical **12** leads to the observed C_1 products (green boxes) whilst dimerization of **12** to oxalate **10** initiates a path to $C_{>1}$ products (orange boxes). Various reactions enable crossing between the C_1 manifold (green background) and the $C_{>1}$ manifold (orange background). The key oxidation of formate **2** back to the carboxyl radical **12** and the slow reduction of **2** that together divert flux from C_1 to $C_{>1}$ products are highlighted (cyan arrows). Photochemical reactions of oxalate **10**, glyoxylate **18** and mesoxalate **23** (purple arrows) also contribute to the network.

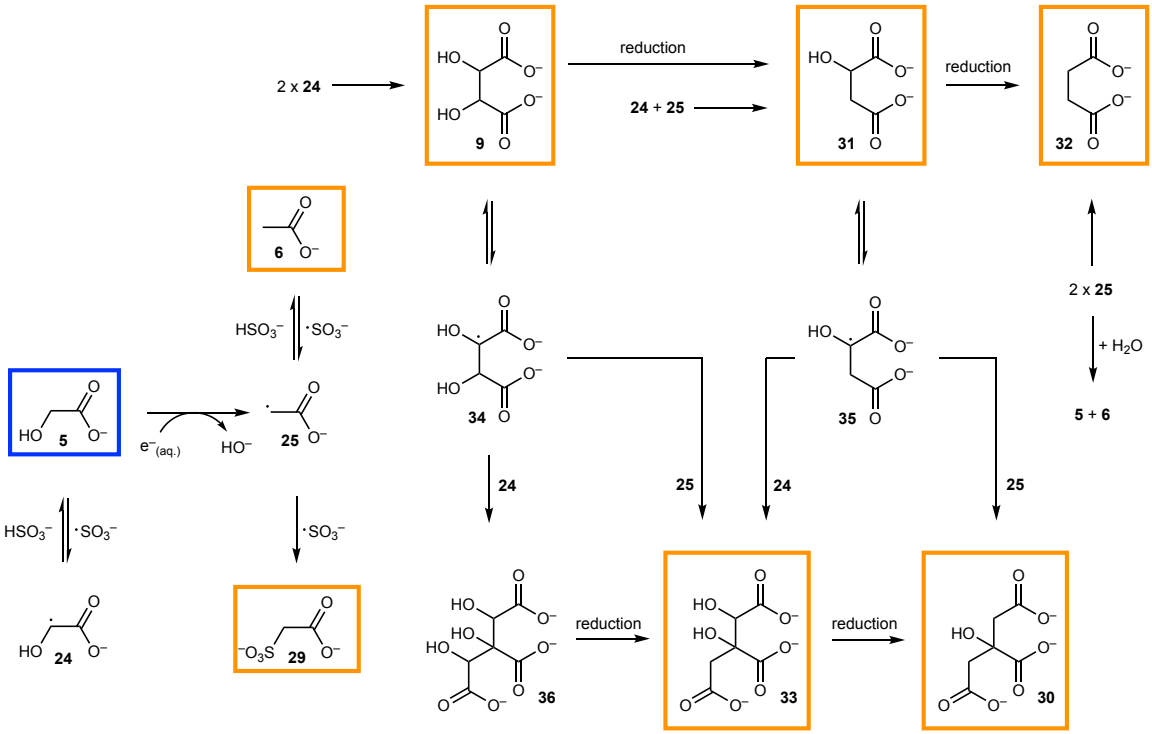

Fig. 2| Carboxysulfitic photoredox reaction network starting from glycolate 5. Glycolate **5** (blue box) can be both oxidized by sulfite radicals and reduced by hydrated electrons to give the radicals **24** and **25** which then react further to give the observed products (orange boxes).

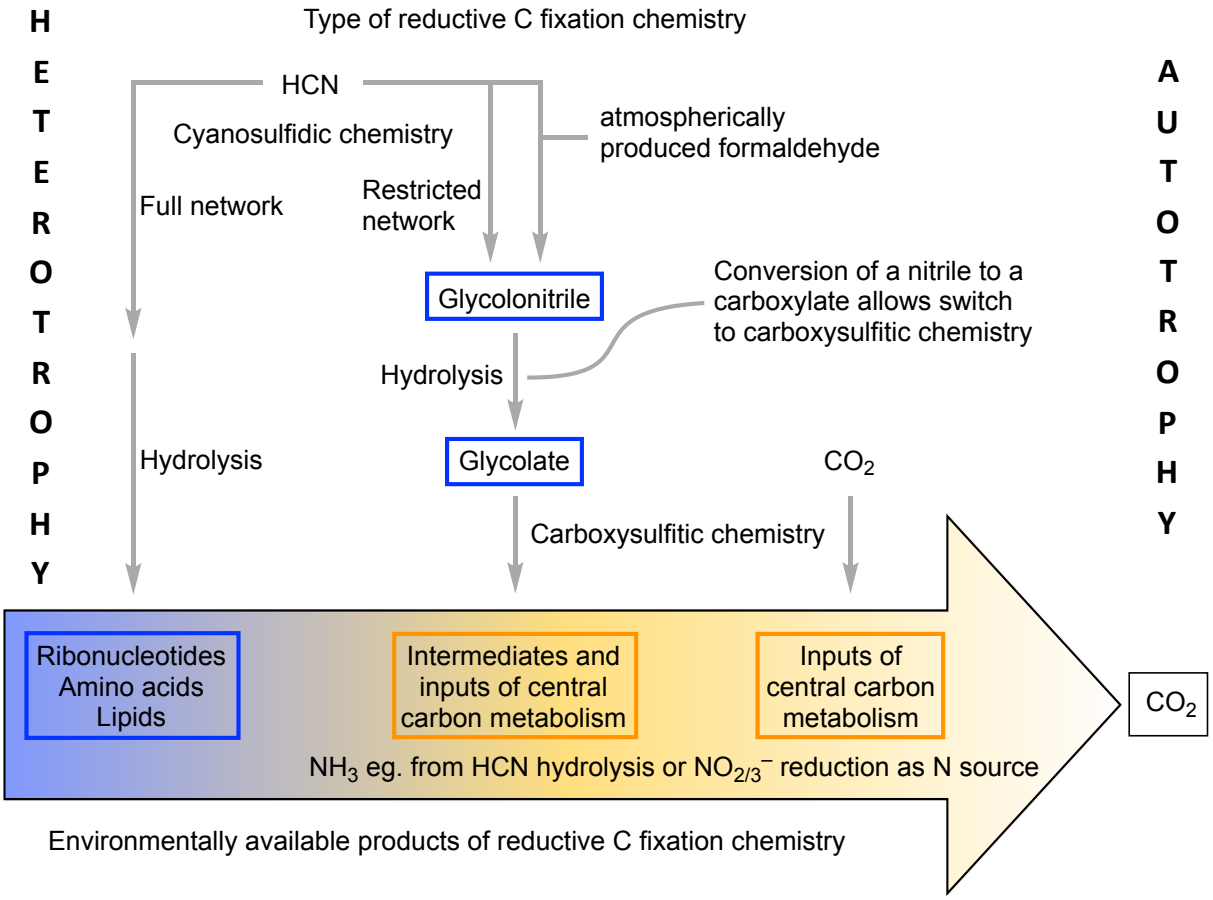

Fig. 3| Connections between environmental chemistry and the development of metabolism. Progression from heterotrophy fed by photochemical products of inorganic carbon reduction to autotrophy as the available products of environmental chemistry become less complex. The preformed building blocks of RNA, peptides and lipids produced by cyanosulfidic chemistry provision the origin and early evolution of life, but gradually become depleted (fading of blue colour in timeline arrow) triggering the development of metabolism starting from simpler but more abundant products derived from glycolate **5** by cyanosulfidic chemistry (dark orange colour in timeline arrow). In turn, these materials become scarce (fading of orange colour in timeline arrow) and biology adapts to using carboxysulfitic products of CO_2 and eventually, CO_2 itself.

Materials and Methods

Materials

All reagents and deuterated solvents used for reactions and spiking experiments were purchased from Sigma-Aldrich and were used without further purification. All photochemical reactions were carried out in *Norell* Suprasil quartz NMR tubes purchased from Sigma-Aldrich using Hg lamps with principal emission at 254 nm in a *Rayonet* photochemical chamber reactor RPR-200, acquired from The Southern New England Ultraviolet Company. StarLab is an in-house constructed photoreactor that delivers broadband UV irradiation to a sample from a xenon lamp[33]. A *Mettler Toledo* SevenEasy pH Meter S20 was used to monitor the pH, and degassed H_2O or D_2O was achieved by four rounds of freeze-pump-thaw cycling. ^{1}H-, and ^{13}C-nuclear magnetic resonance (NMR) spectra were acquired using a *Bruker* Ultrashield 400 Plus or *Bruker* Ascend 400 operating at 400.1, and 100.6 MHz, respectively. Samples consisting of H_2O/D_2O mixtures were analyzed using HOD suppression to collect ^{1}H-NMR data. Chemical shifts (δ) are shown in ppm. Coupling constants (*J*) are given in Hertz and the notations s, d, t represent the multiplicities singlet, doublet, and triplet. The conversion yields were determined by relative integrations of the signals using a known amount of acetamide as internal reference in the ^{1}H-NMR spectrum.

Methods

General method of photoreaction of carboxylates with sulfite

Carboxylates and sodium sulfite (final concentrations were mentioned in Extended Data Table. 1 and Extended Data Table. 2) were dissolved in degassed H_2O/D_2O (9:1, 0.5 mL). After the pH was adjusted to the reported value with NaOH/HCl, the mixture was transferred to a quartz NMR tube which was sealed and irradiated for the reported time (Extended Data Table. 1 and Extended Data Table. 2). The resultant solution was analysed by ^{1}H- and/or ^{13}C-NMR spectroscopy. The yield was calculated by spiking with 4,5-dicyanoimidazole (final concentration of 0.5 mM, 1 mM or 5 mM) and relative integration.

Preparing hydrogen gas in an NMR tube

Metallic zinc (~6 mg) was added to 0.5 mL HCl (0.1 M) aqueous solution. This solution was transferred to an NMR tube after being vortexed for 5 seconds, and was then analysed by ^{1}H-NMR spectroscopy.

Sulfate identification[17]

Sodium bicarbonate (21 mg, 0.25 mmol) and sodium sulfite (63 mg, 0.5 mmol) were dissolved in degassed water (10 mL) and the pH of the resultant solution was adjusted to 9 by adding NaOH/HCl solution. The mixture was then sealed in a quartz tube and irradiated with 254 nm light in the Rayonet photoreactor for 4 hours. 3 mL of the resulting solution was diluted to 20 mL with water and acidified to pH = 1 by the addition of concentrated HCl. The acidified solution was heated to nearly boiling for at least 30 min to remove all carbon dioxide and sulfur dioxide. Barium chloride solution was then added to the solution to give a precipitate which persisted upon boiling for another 30 min. The precipitate did not dissolve in dilute HCl solution.

Ultrafast pump-probe experiments

The general principles of pump-probe spectroscopy are described in the following references[49-51]. The fundamental of the excitation pulses (800 nm) was generated by a Ti:Sa

based laser-amplifier system (Solstice Ace by Spectra-Physics, Newport Co.) with a repetition rate of 1 kHz and a pulse duration of ~90 fs. The excitation pulses (251 nm) were generated in a nonlinear amplifier system (Topas Prime + NIRUVis, Light Conversion, Ltd.) and stretched by a 25 cm fused silica block (Corning) to ~ 1.7 ps to suppress two-photon ionization of the solvent. The excitation energy at the sample position was ~1 μJ and the spot diameter of ~250 μm (fwhm). For our *microsecond* ultrafast pump-probe spectroscopy (Table S2) the broadband probe light (unpolarized) was generated, delayed, and detected in an EOS Fire system (Ultrafast Systems, LLC), with a nominal spectral range of 350 – 950 nm. For our *picosecond* ultrafast pump-probe spectroscopy (Figure S29) the broadband probe light was generated, delayed, and detected in a HELIOS Fire system (Ultrafast Systems, LLC), with a nominal spectral range of 400 – 750 nm. These spectral ranges are ideal for monitoring the broad absorption feature of the hydrated electron, which is centered near 700 nm. The experiments were carried out at a temperature of 23°C.

The transient pump-probe data were cropped to the spectral range 450 nm – 913 nm and 20 adjacent channels were averaged (Surface Xplorer, Ultrafast Systems, LLC). A global fitting analysis to determine transient lifetimes was performed[52-54].

References

49. Schrader, T. et al. Vibrational relaxation following ultrafast internal conversion: comparing IR and Raman probing. *Chem. Phys. Lett.* **392**, 358–364 (2004).

50. Ryseck, G. et al. The Excited-State Decay of 1-Methyl-2(1*H*)-pyrimidinone is an Activated Process. *ChemPhysChem* **12**, 1880–1888 (2011).

51. Haiser, K. et al. Mechanism of UV-induced formation of Dewar lesions in DNA. *Angew. Chem. Int. Ed.*, **51**, 408–411 (2012).

52. Satzger, H. & Zinth, W., Visualization of transient absorption dynamics – towards a qualitative view of complex reaction kinetics. *Chem. Phys.,* **295**, 287–295 (2003).

53. Dominguez, P. N., Himmelstoss, M., Michelmann, J., Lehner, F. T., Gardiner, A. T., Cogdell, R. J., & Zinth, W. Primary reactions in photosynthetic reaction centers of Rhodobacter sphaeroides–Time constants of the initial electron transfer. *Chem. Phy. Lett.,* **601**, 103-109. (2014).

54. Gutierrez-Osuna, R., Nagle, H. T., & Schiffman, S. S. Transient response analysis of an electronic nose using multi-exponential models. *Sens. Actuators B Chem.,* **61**, 170-182 (1999).

Extended Data Table. 1 | Product concentrations and percentage yields after UV irradiation of solutions of $NaHCO_3$ and Na_2SO_3.

Entry	[$NaHCO_3$] /mM	[Na_2SO_3] /mM	**2**[a]	**3**	**4**	**5**	**6**	**7**	**8**	**9a**	**9b**	**11**	**29**	**37**	Time
1	5	10	0.03 0.6 %			20 0.8 %	10 0.4 %	120 7.2 %	30 1.8 %						4 h
2	20	40	3.7 19 %		40 0.2 %	100 1.0 %	20 0.2 %	600 9.0 %	200 3.0 %						4 h
3	50	100	18.0 36 %	200 0.4 %	200 0.4 %	200 0.8 %	50 0.2 %	600 3.6 %	300 1.8 %	30 0.24 %	30 0.24 %				4 h
4	100	200	27.6 28 %	500 0.5 %	120 0.1 %	20 0.04 %	20 0.04 %	150 0.5 %	40 0.12 %						4 h
5	100	200	52.7 53 %	200 0.2 %	4600 4.6 %	300 0.6 %	300 0.6 %	500 1.5 %	900 2.7 %	30 0.12 %	20 0.08 %	100 0.3 %			24 h
6[b]	5	4 x 10	0.03 0.6%			20 0.8%	27 1.0%	110 6.6%	270 16.2%				20 0.8%		4 x 1h
7[c]	5	50	1.6 32 %	15 0.3 %	143 2.9 %	12 0.5 %	8 0.3 %	59 3.5 %	102 6.1 %				8 0.3 %	45 1.8 %	168 h

a. Concentration of formate **2** in mM, concentrations of other products in μM. b. The concentration of sodium bicarbonate was 5 mM with 10 mM sodium sulfite initially followed by additional 10 mM sodium sulfite hourly (40 mM total). c. Using a lower intensity broadband lamp source (StarLab).

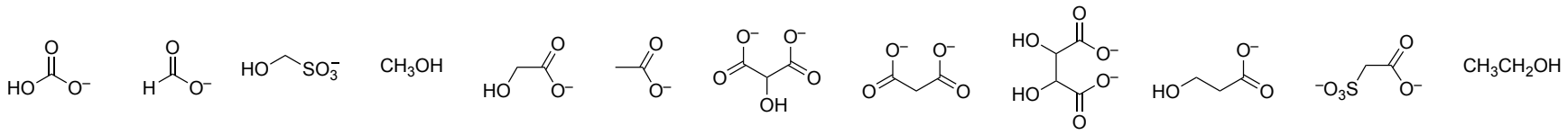

1 **2** **3** **4** **5** **6** **7** **8** **9** **11** **29** **37**

Extended Data Table. 2 | Product concentrations and percentage yields after irradiation of individual bicarbonate reduction products (50 mM) and Na_2SO_3 (100 mM).

Entry	Cpd.	**2**[a]	**3**	**4**	**5**	**6**	**7**	**8**	**9a**	**9b**	**11**	**29**	**30**	**31**	**32**	**33**	**37**	Time
1	**2**		1900 3.8 %	3300 6.6 %	300 1.2 %	240 1.0 %	340 2.0 %	550 3.3 %				70 0.28 %						4 h
2	**3**	6.9 14 %		12700 25.0 %		600 2.4 %												7 h
3	**4**	1.4 2.8 %	2300 4.6 %			273 1.09 %											1580 6.32 %	6 h
4	**5**[b]			10 0.1 %		1000 20 %		40 1.2 %	380 15 %	190 7.6%		810 16 %	15 0.9 %	390 15.6 %	70 2.8 %			2 h
5	**5**	0.6 0.6 %	700 0.7 %	150 0.15 %		16200 32 %		100 0.3 %	1500 6 %	1000 4 %		8000 16 %	200 1.2 %	3000 12 %	1070 4.4 %	190 1.1 %		6 h
6	**5**[c]	0.7 0.7 %	400 0.4 %	20 0.02 %		1700 3.4 %			400 1.6 %	400 1.6 %		200 0.4 %		200 0.8 %				8 h
7	**5**[c,d]	0.89 8.9 %	35 0.35 %	40 0.4 %		356 7.12 %		15 0.45 %	210 8.4 %	105 4.2 %	50 1.5%	130 2.6 %		50 2.0 %	5 0.2%			144 h
8	**6**			40 0.04 %	100 0.2 %			30 0.09 %				1600 3.2 %			90 0.36 %		480 0.96 %	6 h
9	**7**	2.4 1.6 %			400 0.53 %	1000 1.3 %	-	24300 48.6 %	N.d.[e]	120 0.3 %	800 1.6 %	400 0.5 %						7 h
10	**8**	0.4 0.3 %				200 0.3 %		-			2000 4.0 %							2 h
11	**9**	9.2 9.2 %		40 0.04 %	3700 7.4 %	100 0.2 %	200 6.0 %	50 0.15 %	1100 4.4 %	1100 4.4 %				300 1.2 %				6 h

a. Concentration of product formate **2** in mM, concentrations of other products in μM. b. The concentration of glycolate **5** was 5 mM with 10 mM sodium sulfite. c. Using a lower intensity broadband lamp source (StarLab). d. The concentration of glycolate **5** was 5 mM with 50 mM sodium sulfite. e. Not distinguishable, ^{1}H-NMR signal obscured by the signal for starting material **7**.

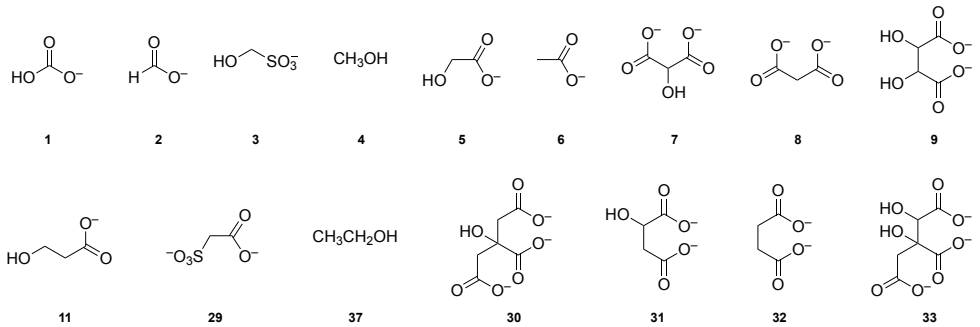

Supplementary Information

Prebiotic photoredox synthesis from carbon dioxide and sulfite

Ziwei Liu[1], Long-Fei Wu[1], Corinna Kufner[2], Dimitar D. Sasselov[2], Woodward W. Fischer[3] and John D. Sutherland[1]*

[1]MRC Laboratory of Molecular Biology, Francis Crick Avenue, Cambridge Biomedical Campus, Cambridge, CB2 0QH, UK. [2]Harvard-Smithsonian Center for Astrophysics, Cambridge, Massachusetts, MA 02138, USA. [3]Division of Geological and Planetary Sciences, California Institute of Technology, Pasadena, CA 91125, USA.

*Correspondence to: johns@mrc-lmb.cam.ac.uk

Figures S1 to S29, Tables S1 to S2.

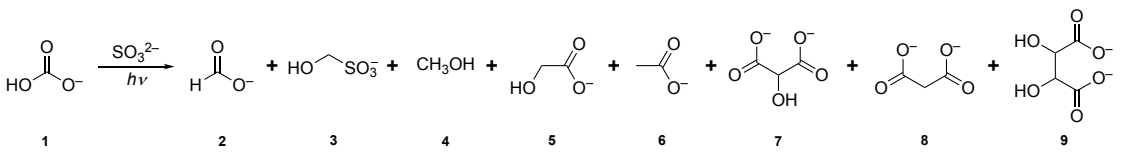

573

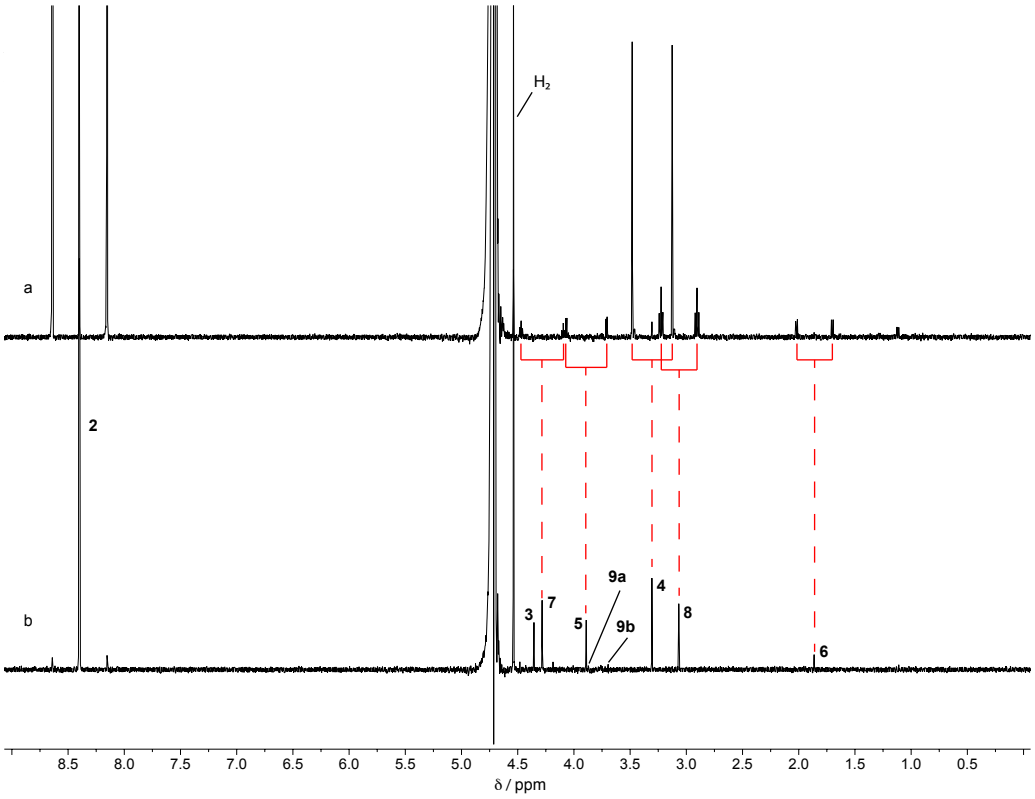

574

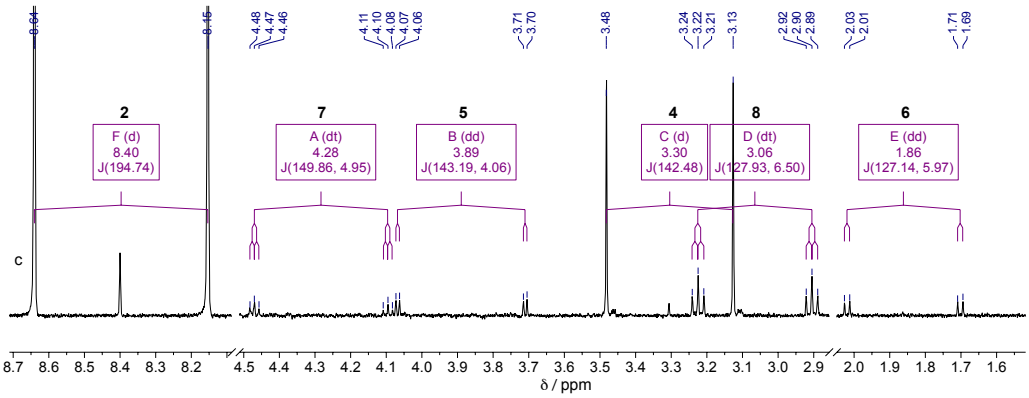

575

576 **Fig. S1.**

577 Stacked ^{1}H-NMR spectra of: a) a solution of NaH^{13}CO$_3$ ^{13}C-**1** (50 mM) and Na$_2$SO$_3$ (150 mM) at
578 pH = 9 after irradiation for 24 hours showing all product ^{1}H signals split by ^{13}C-^{1}H coupling;
579 b) a solution of NaHCO$_3$ **1** (50 mM) and Na$_2$SO$_3$ (100 mM) at pH = 9 after irradiation for 4
580 hours; c) Expansion of the spectrum shown in a) showing signal splitting and coupling constants
581 (/Hz).

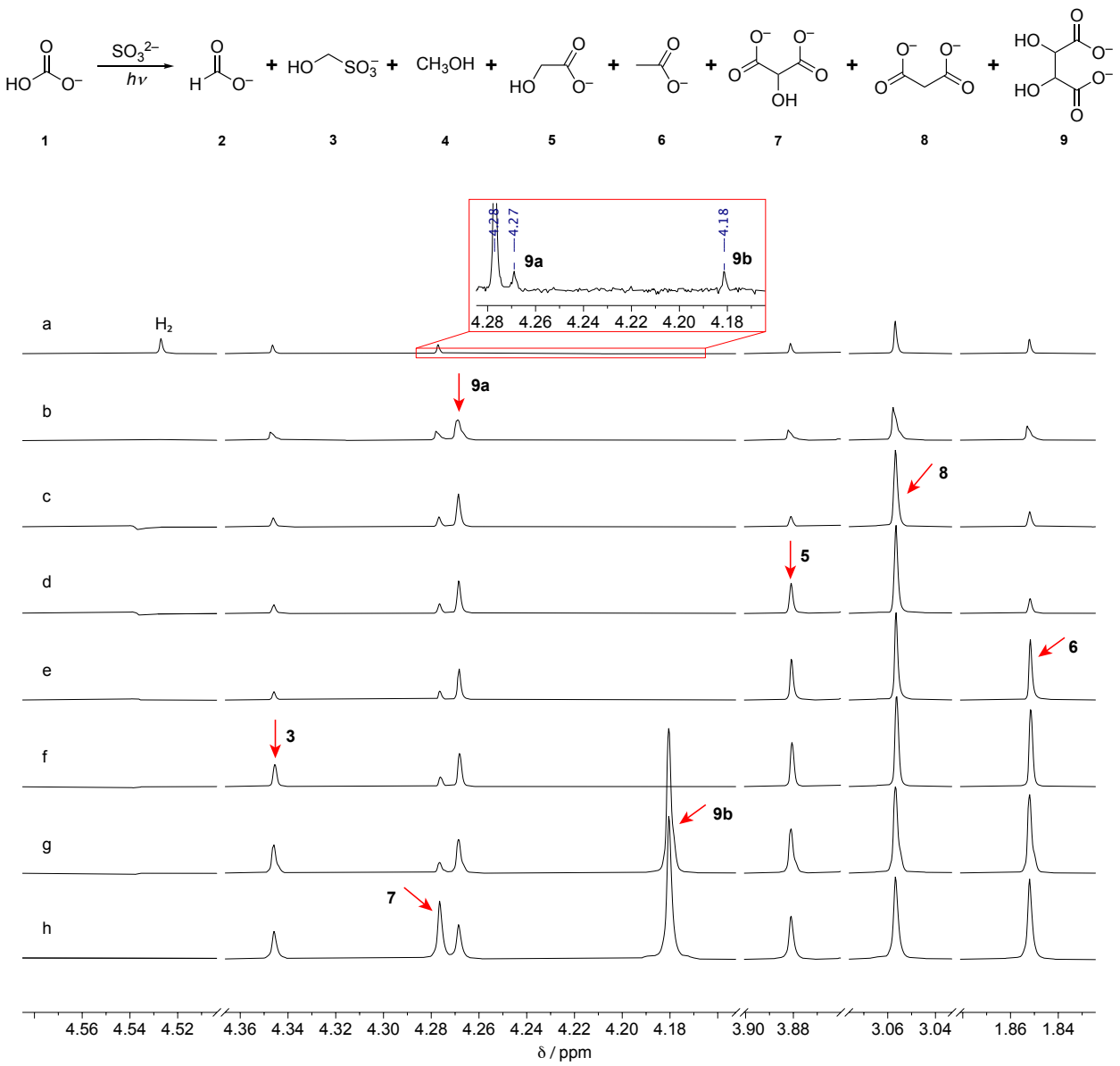

Fig. S2.

Stacked ^{1}H-NMR spectra of the reaction mixture before and after sequential spiking with authentic samples. a) $NaHCO_3$ **1** (50 mM), Na_2SO_3 (100 mM) at pH = 9 after irradiation for 4 hours; b) + L-tartrate **9a**; c) + malonate **8**; d) + glycolate **5**; e) + acetate **6**; f) + hydroxymethanesulfonate **3**; g) + *meso*-tartrate **9b**; h) + tartronate **7**.

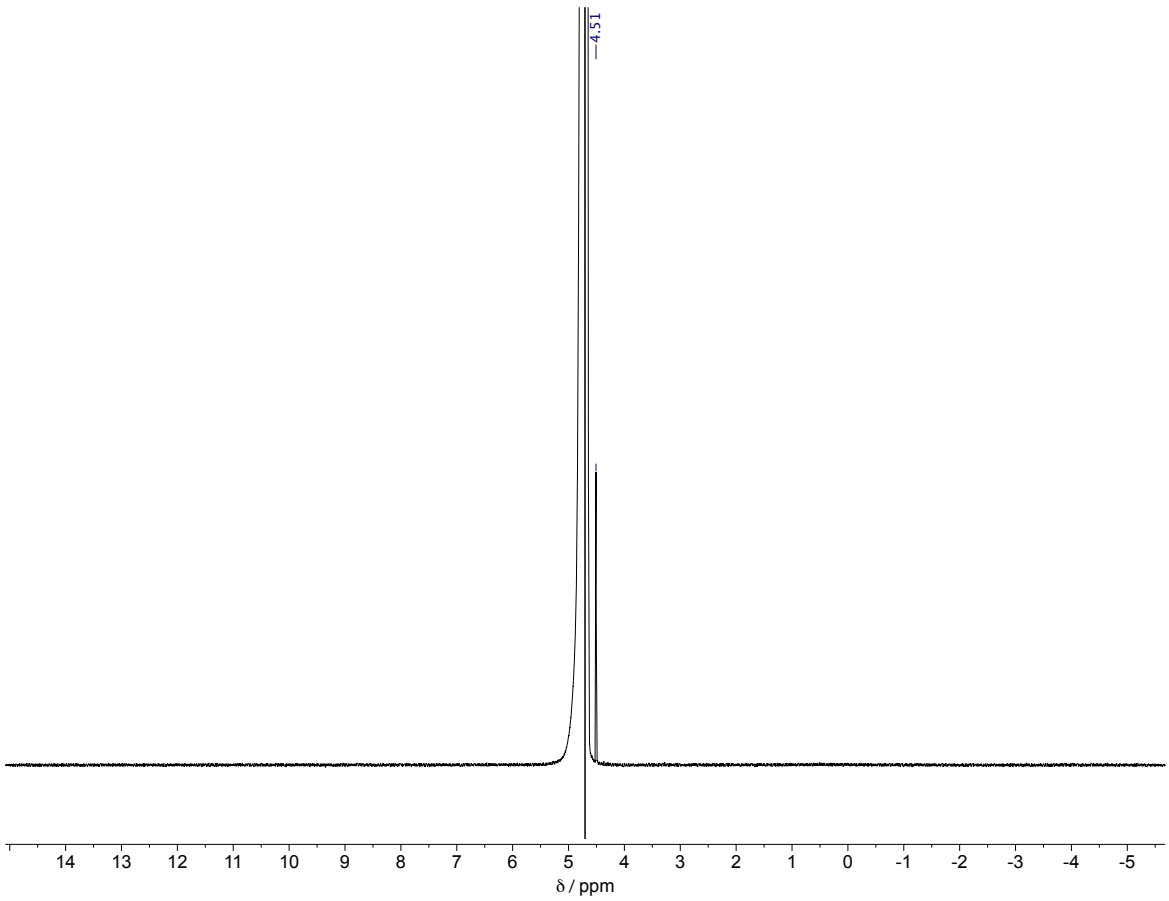

Fig. S3.

^{1}H-NMR spectrum of the reaction products after treating zinc (6 mg) with hydrochloric acid (100 mM) for 1 hour showing a signal for H_2 at $\delta = 4.5$ ppm.

595

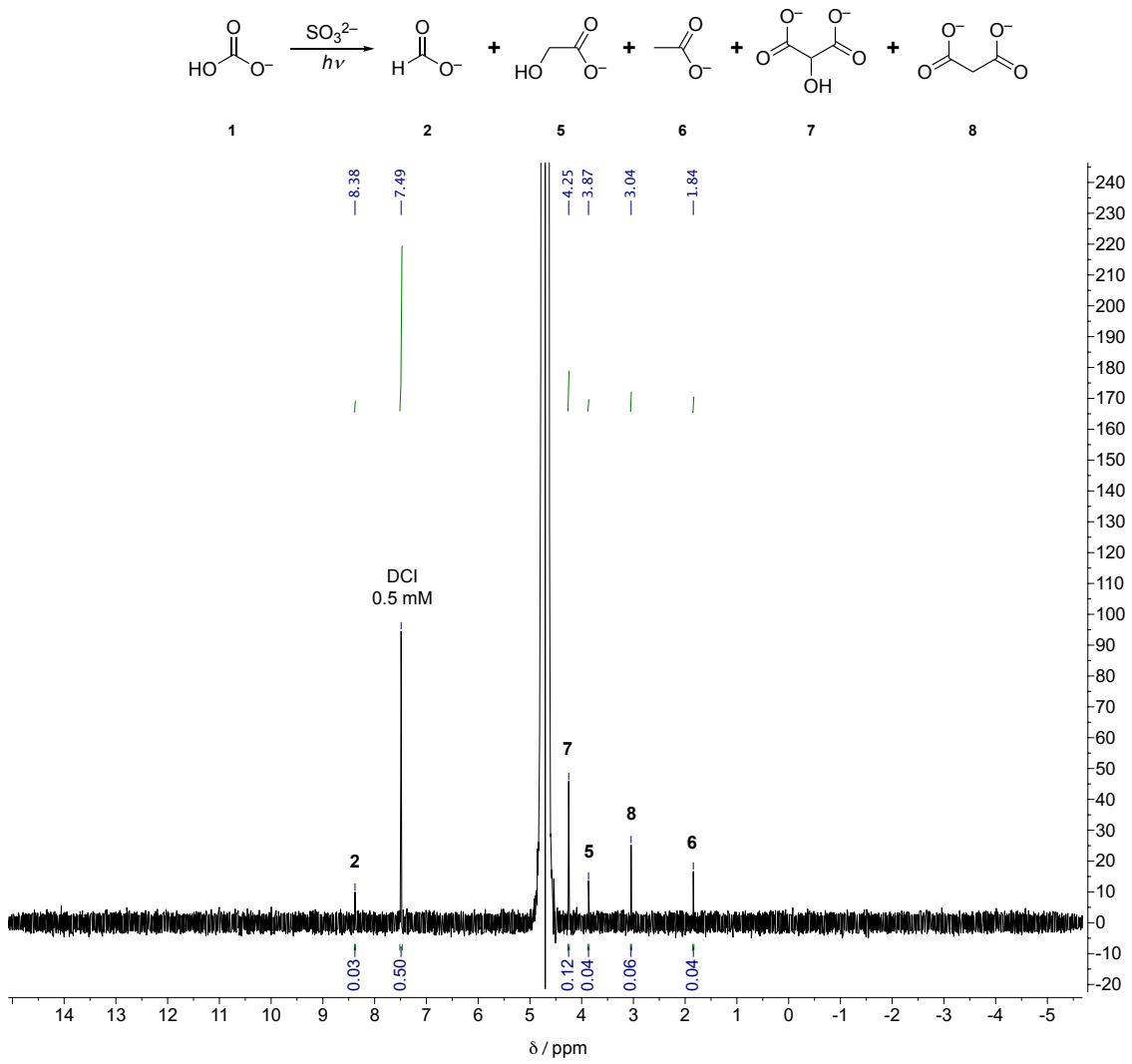

596

597 **Fig. S4.**

598 ^{1}H-NMR spectrum of the reaction products of $NaHCO_3$ **1** (5 mM), Na_2SO_3 (10 mM) at pH = 9
599 after irradiation for 4 hours, with 4,5-dicyanoimidazole (DCI, 0.5 mM) added after the reaction
600 as an internal standard.

601

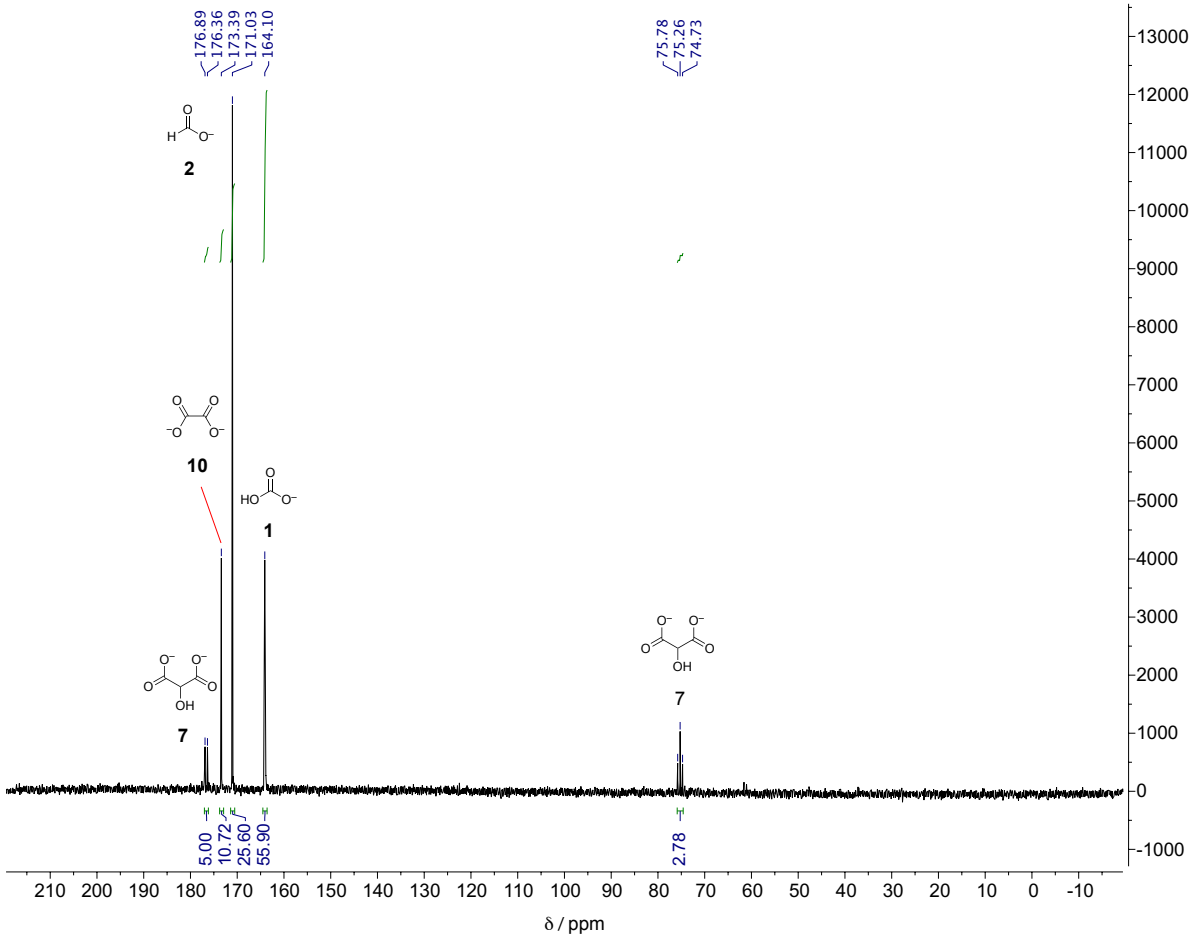

Fig. S5.
Quantitative ^{13}C-NMR spectrum showing the production of oxalate **10** in ~11% yield after irradiation of a solution containing $NaH^{13}CO_3$ ^{13}C-**1** (5 mM) and Na_2SO_3 (10 mM) (pH = 9 before irradiation) for 1 hour followed by addition of further Na_2SO_3 (10 mM) and irradiation for an additional 1 hour. Assignment by comparison to spectrum of an authentic standard.

610

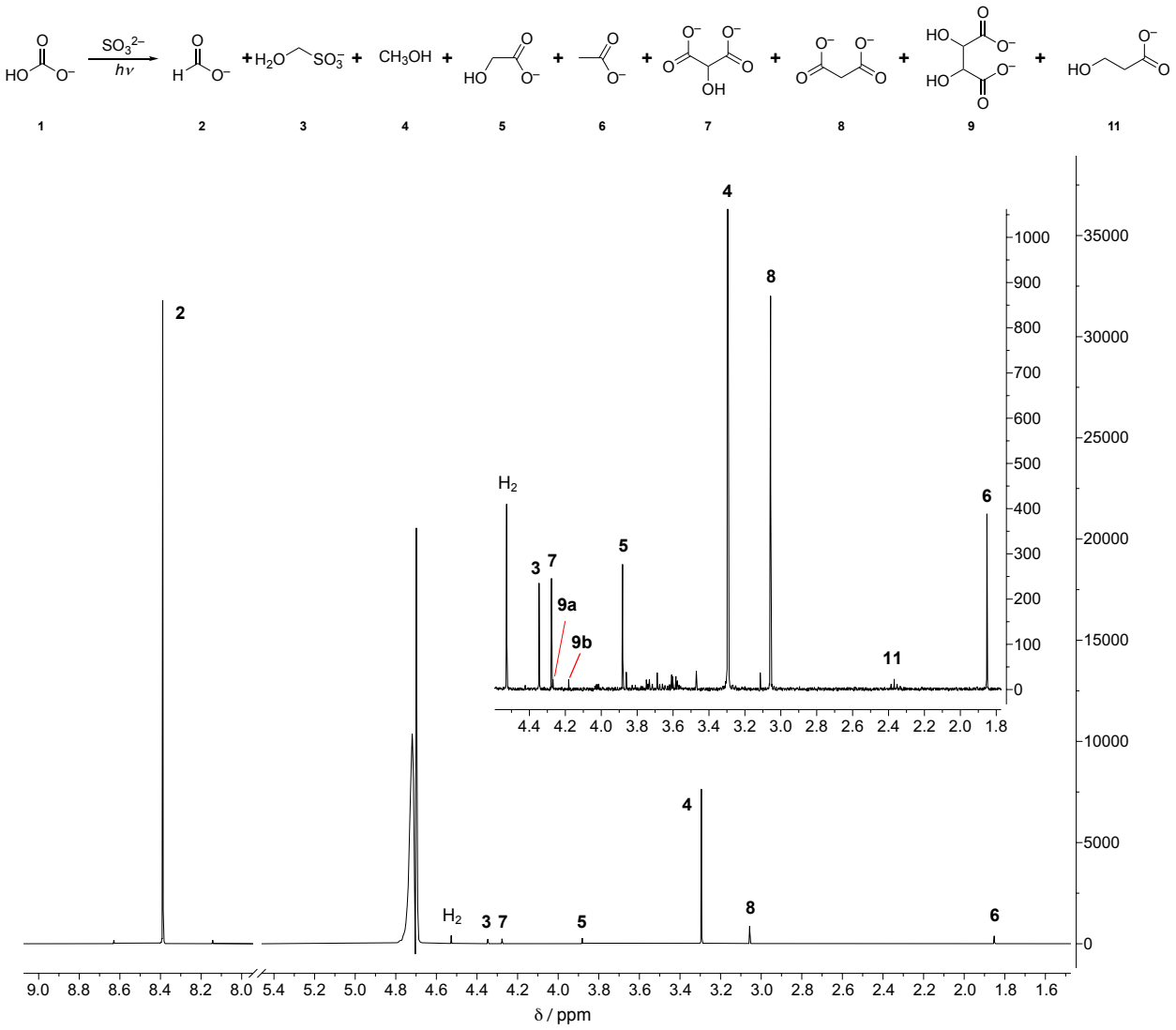

611

612 **Fig. S6.**

613 ^{1}H-NMR spectrum of the reaction products of $NaHCO_3$ **1** (100 mM), Na_2SO_3 (200 mM) at pH =
614 9 after irradiation for 24 hours.

615

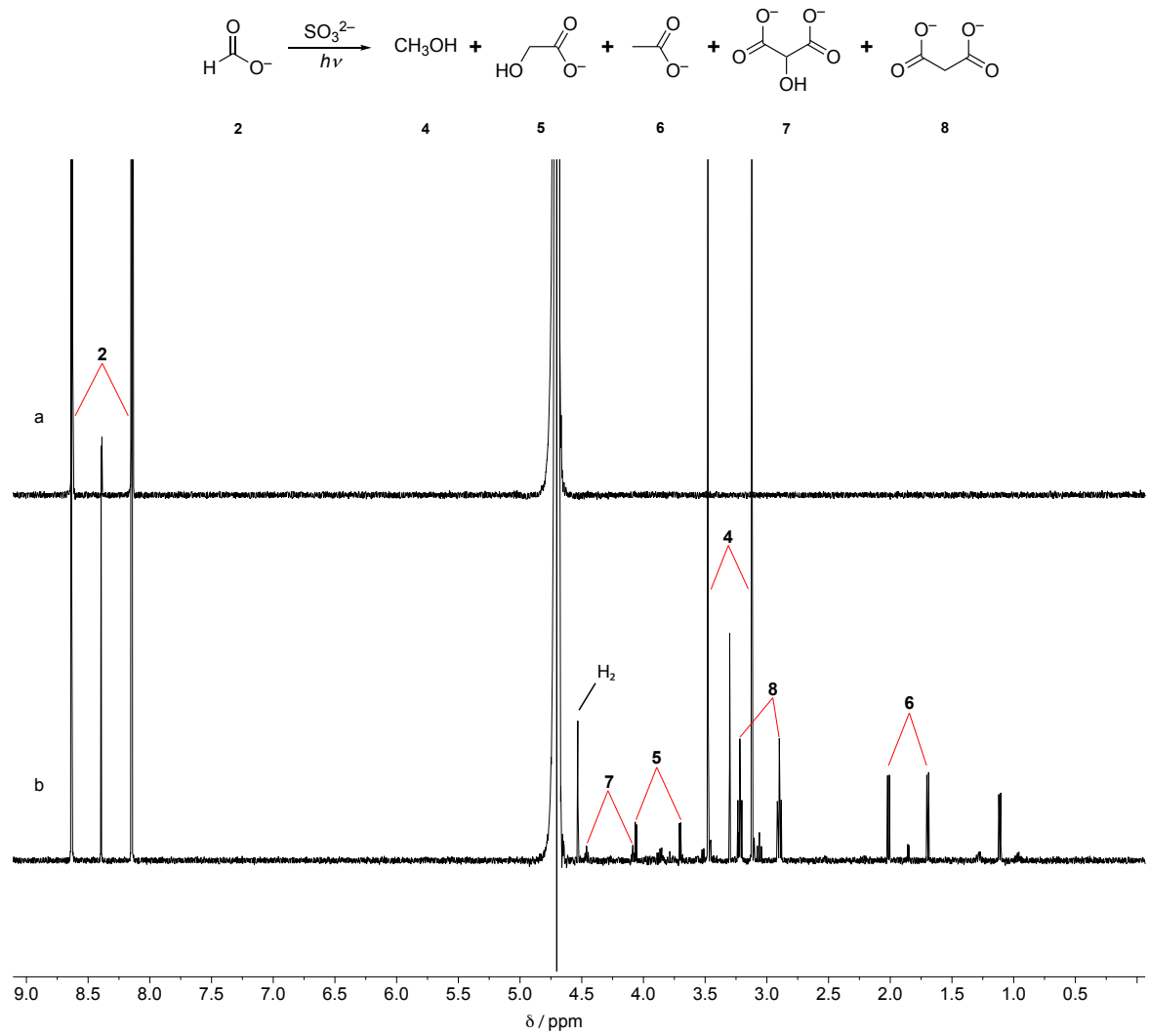

Fig. S7.

Stacked ^{1}H-NMR spectra of a solution of ^{13}C-labelled sodium formate ^{13}C-**2** (50 mM) and Na_2SO_3 (100 mM) at pH = 9, a) before irradiation; b) after 24 hours irradiation showing all product ^{1}H signals split by ^{13}C-^{1}H coupling.

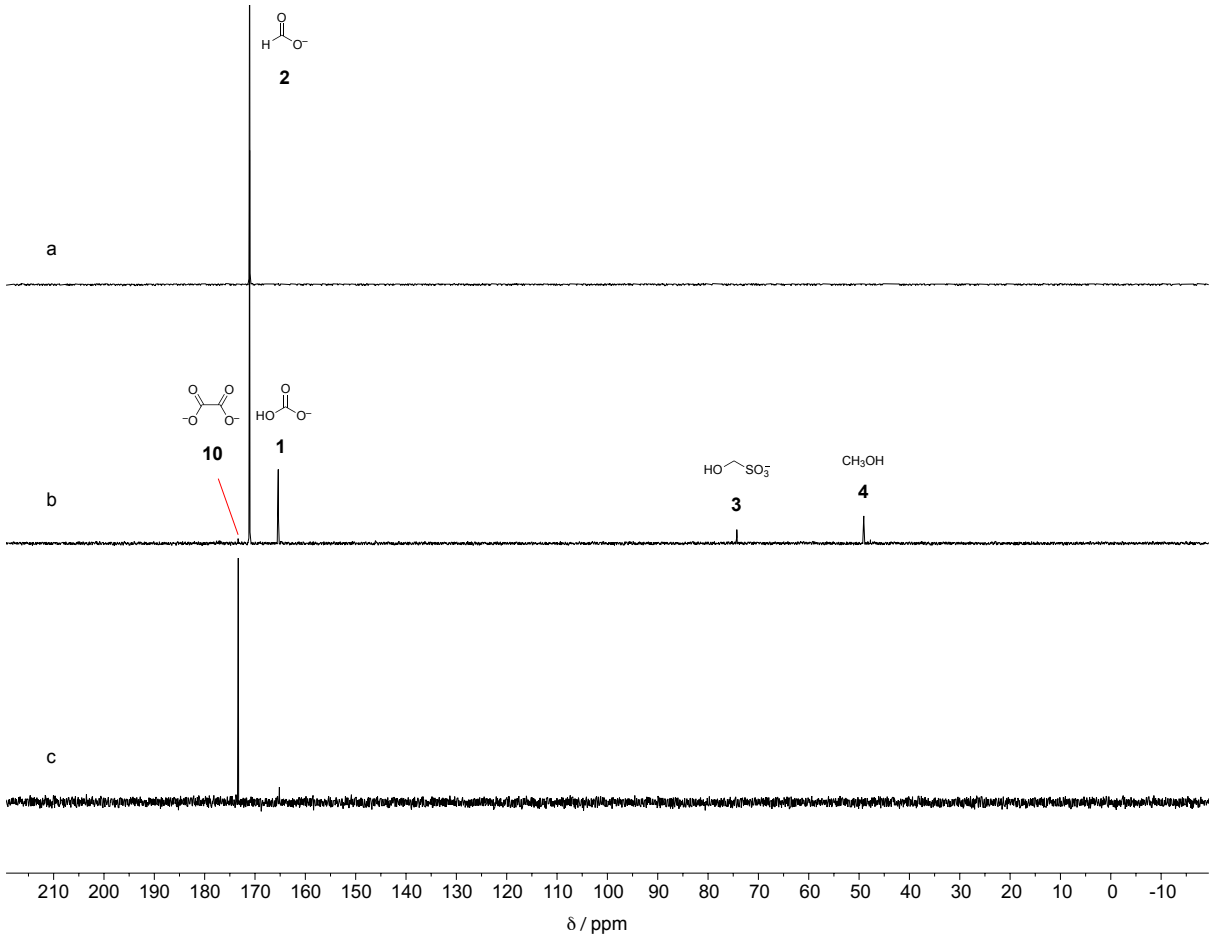

Fig. S8.

Stacked ^{1}H-NMR spectra of a solution of ^{13}C-labelled sodium formate ^{13}C-**2** (50 mM) and Na_2SO_3 (100 mM) at pH = 9, a) before irradiation; b) after 24 hours irradiation showing all product; c) authentic oxalate standard.

629

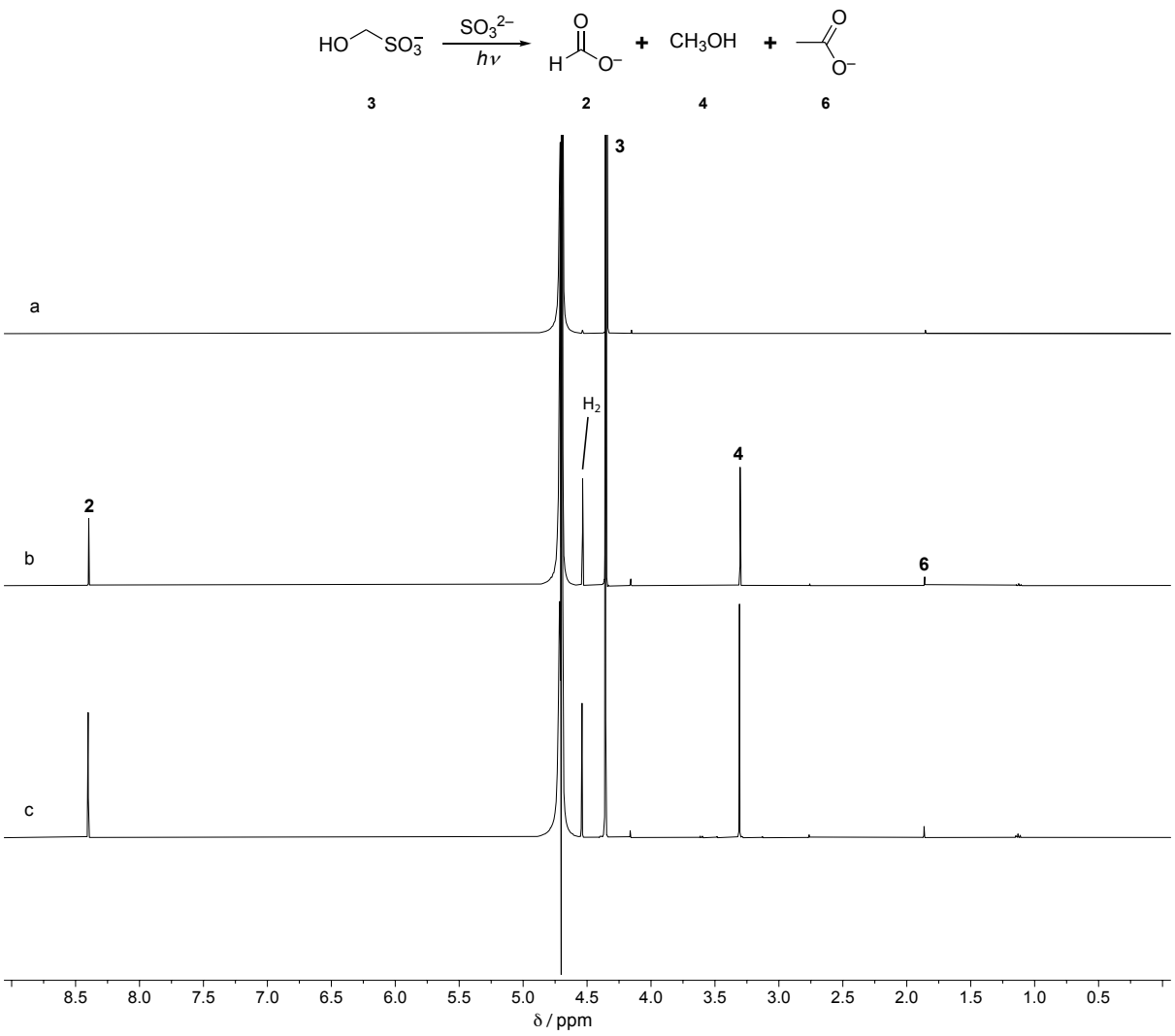

630

631 **Fig. S9.**

632 Stacked ^{1}H-NMR spectra of a solution of sodium hydroxymethanesulfonate **3** (50 mM) and
633 Na_2SO_3 (100 mM) at pH = 9, a) before irradiation; b) after 2 hours irradiation; c) after 7 hours
634 irradiation.

635

636

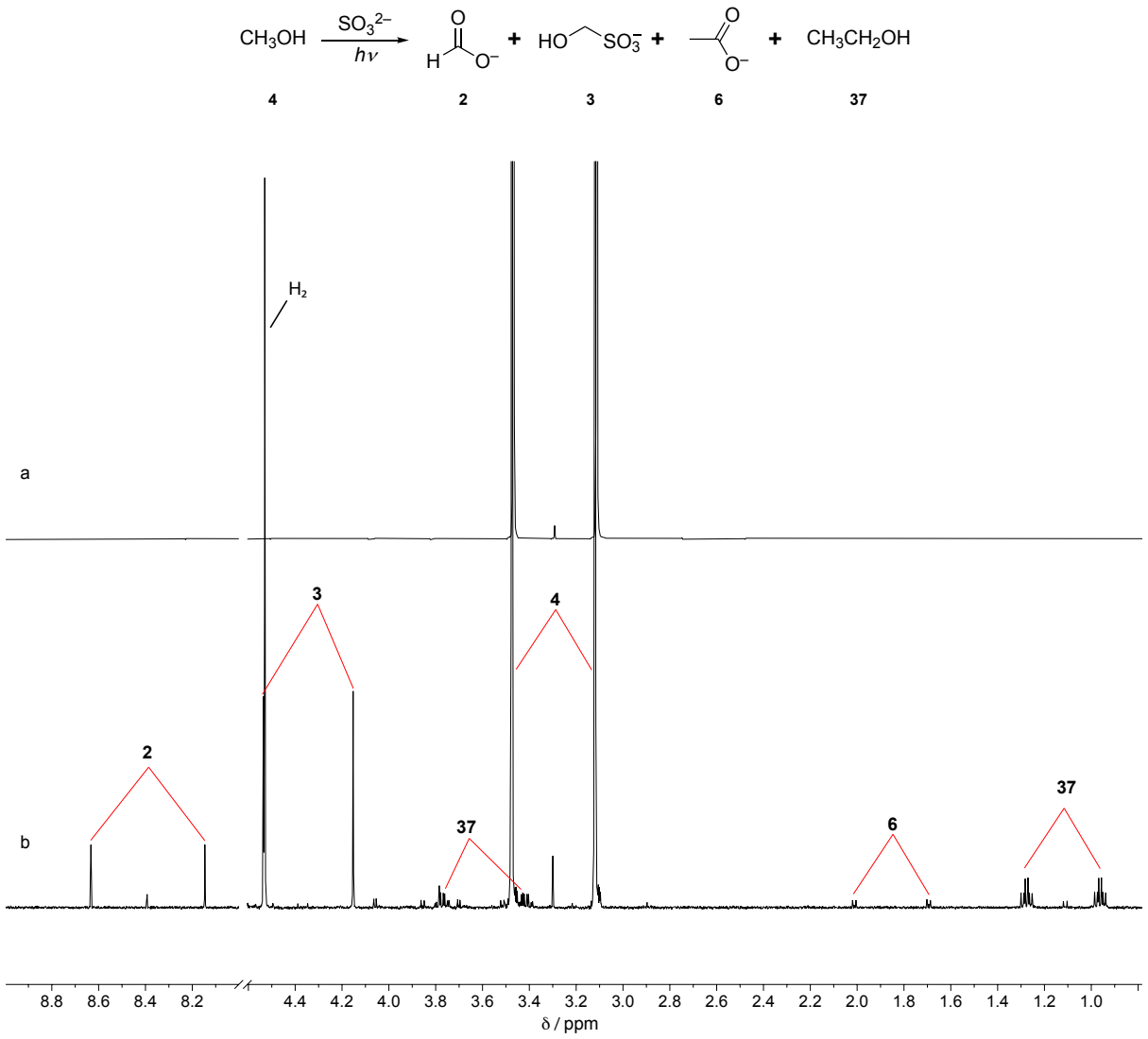

637

638 **Fig. S10.**

639 Stacked ^{1}H-NMR spectra of a solution of ^{13}C-labelled methanol ^{13}C- **4** (50 mM) and Na_2SO_3
640 (100 mM) at pH = 9, a) before irradiation; b) after 6 hours irradiation showing all product ^{1}H
641 signals split by ^{13}C-^{1}H coupling.

642

643

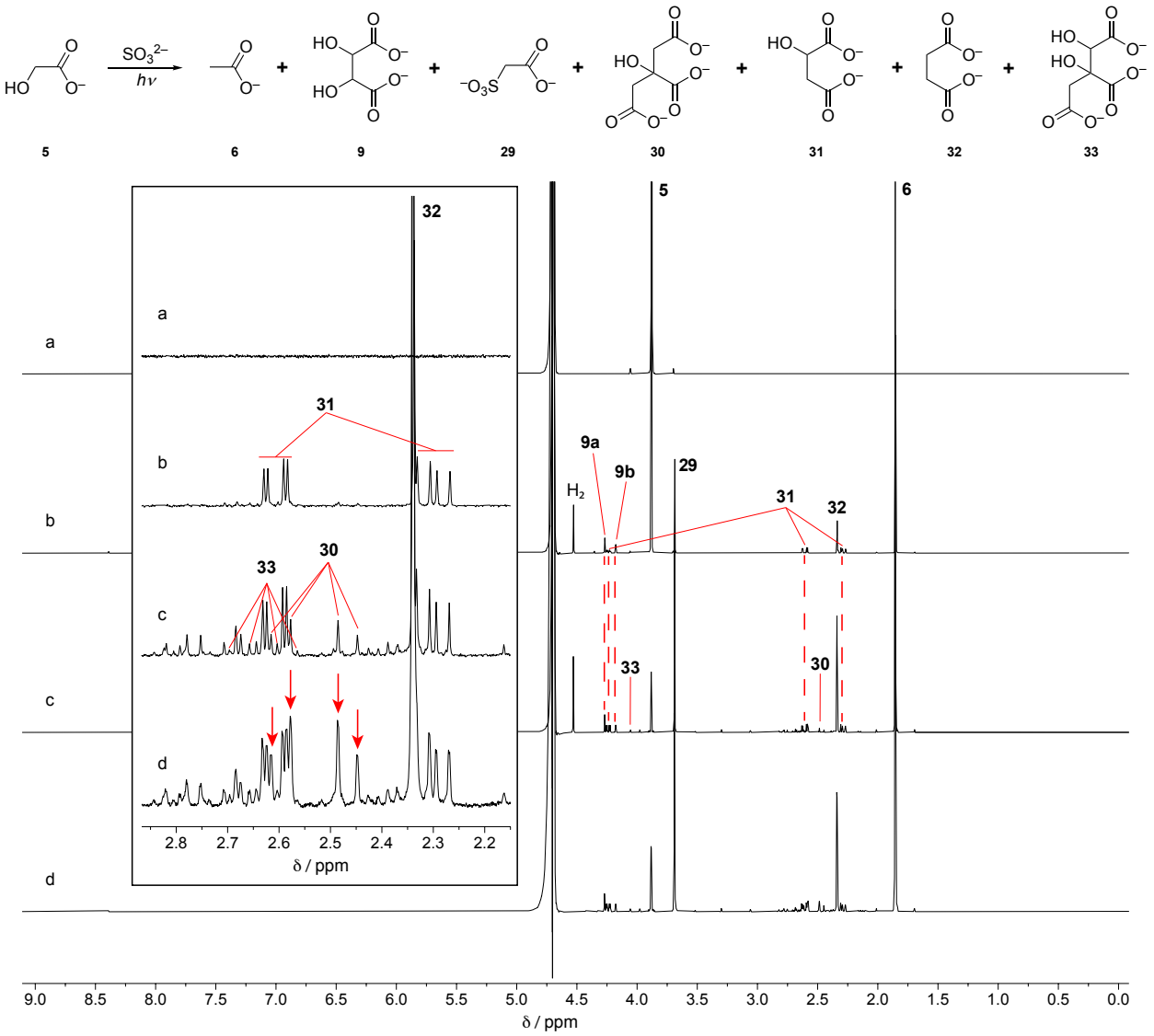

644

645 **Fig. S11.**

646 Stacked ^{1}H-NMR spectra of a solution of sodium glycolate **5** (50 mM) and Na_2SO_3 (100 mM) at
647 pH = 9, a) before irradiation; b) after 2 hours irradiation; c) after 6 hours irradiation; d) same as
648 c) after spiking with authentic citrate **30**.

649

650

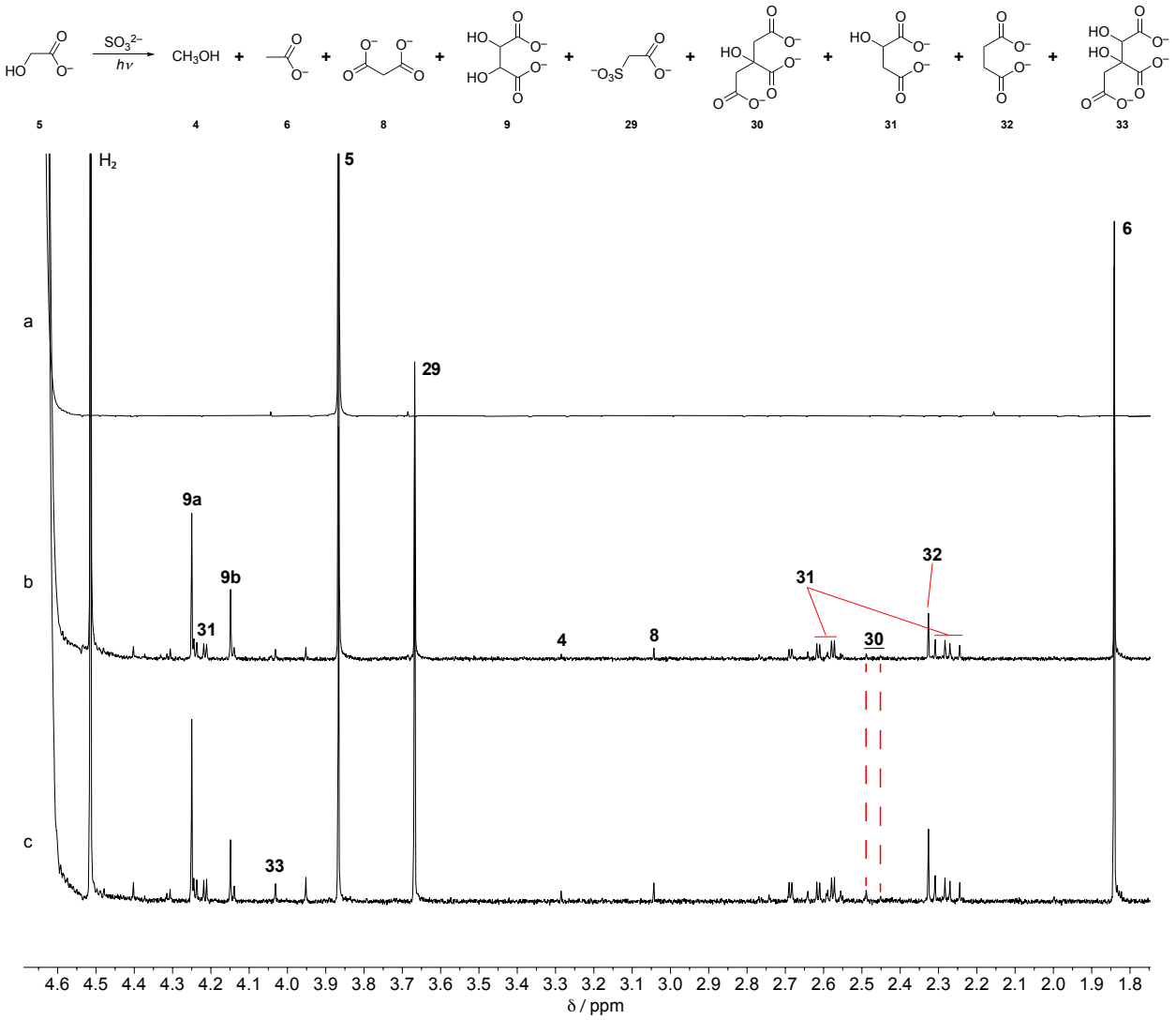

651

652 **Fig. S12.**

653 Stacked ^{1}H-NMR spectra of a solution of sodium glycolate **5** (5 mM) and Na_2SO_3 (100 mM) at
654 pH = 9, a) before irradiation; b) after 2 hours irradiation; c) after 4 hours irradiation.
655

656

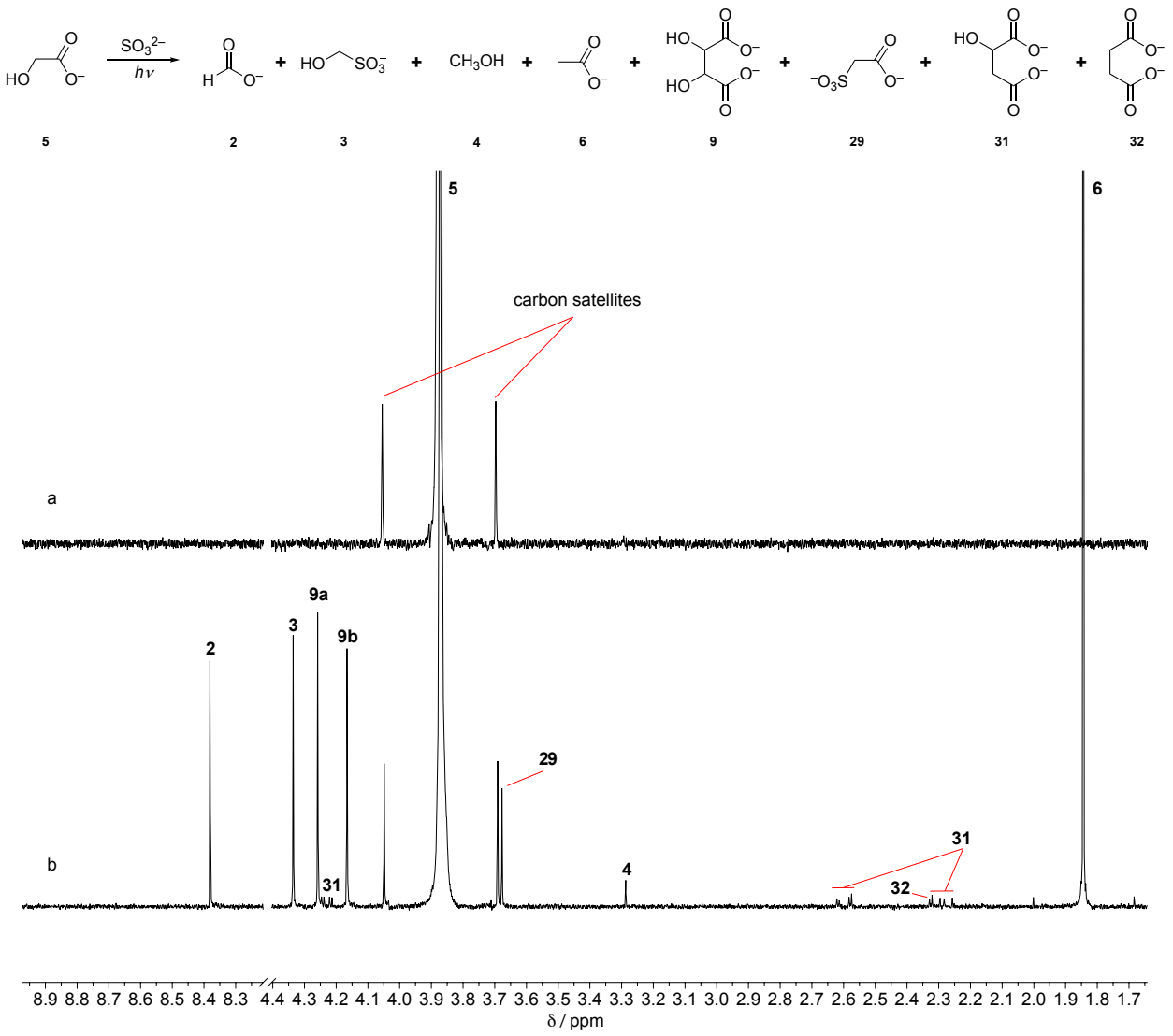

657

658 **Fig. S13.**

659 Stacked ^{1}H-NMR spectra of a solution of sodium glycolate **5** (50 mM) and Na_2SO_3 (100 mM) at
660 pH = 9, a) before irradiation; b) after 8 hours broadband UV irradiation in the StarLab apparatus.
661

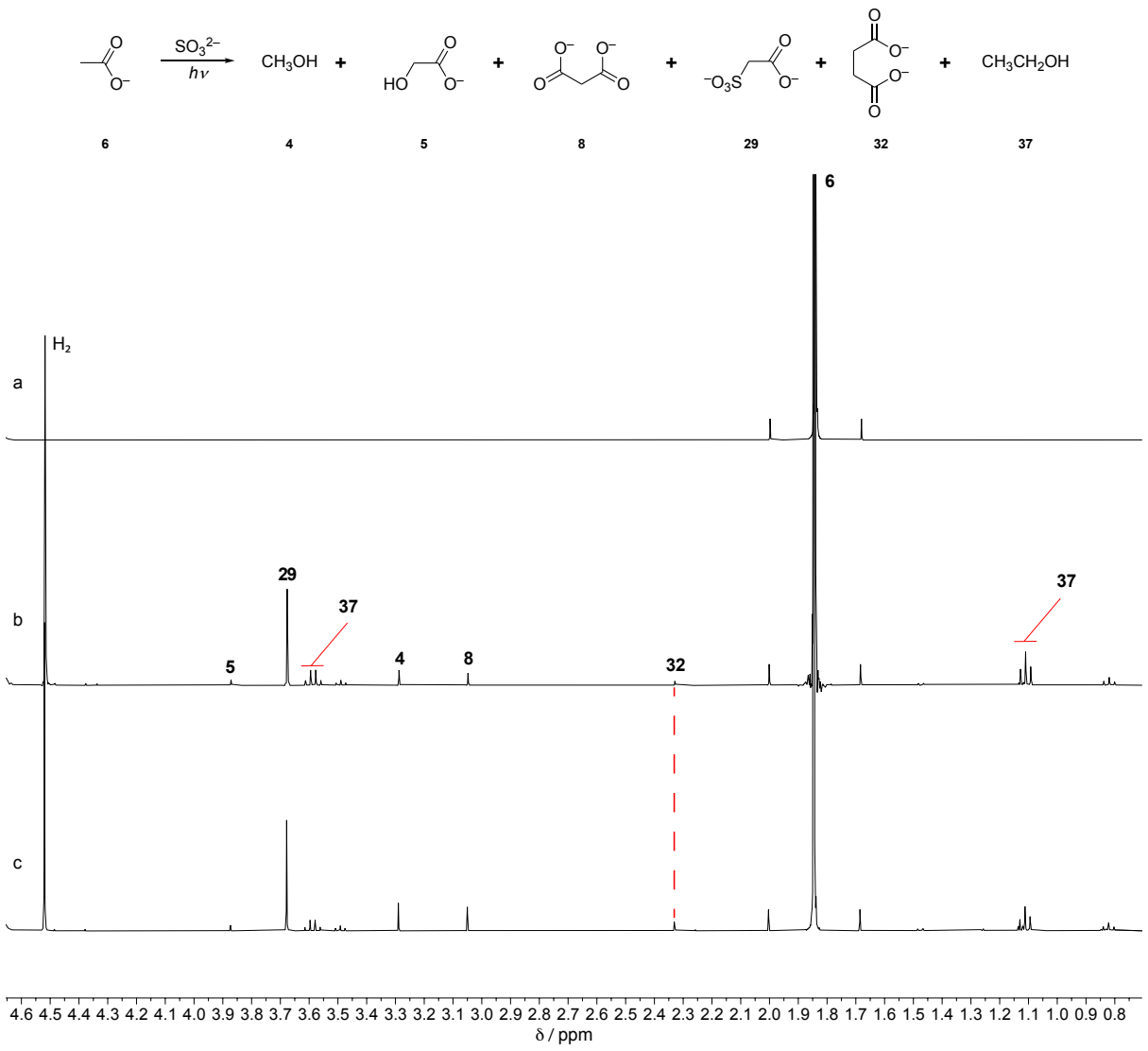

Fig. S14.

Stacked ^{1}H-NMR spectra of a solution of sodium acetate **6** (50 mM) and Na_2SO_3 (100 mM) at pH = 9, a) before irradiation; b) after 2 hours irradiation; c) after 6 hours irradiation.

668

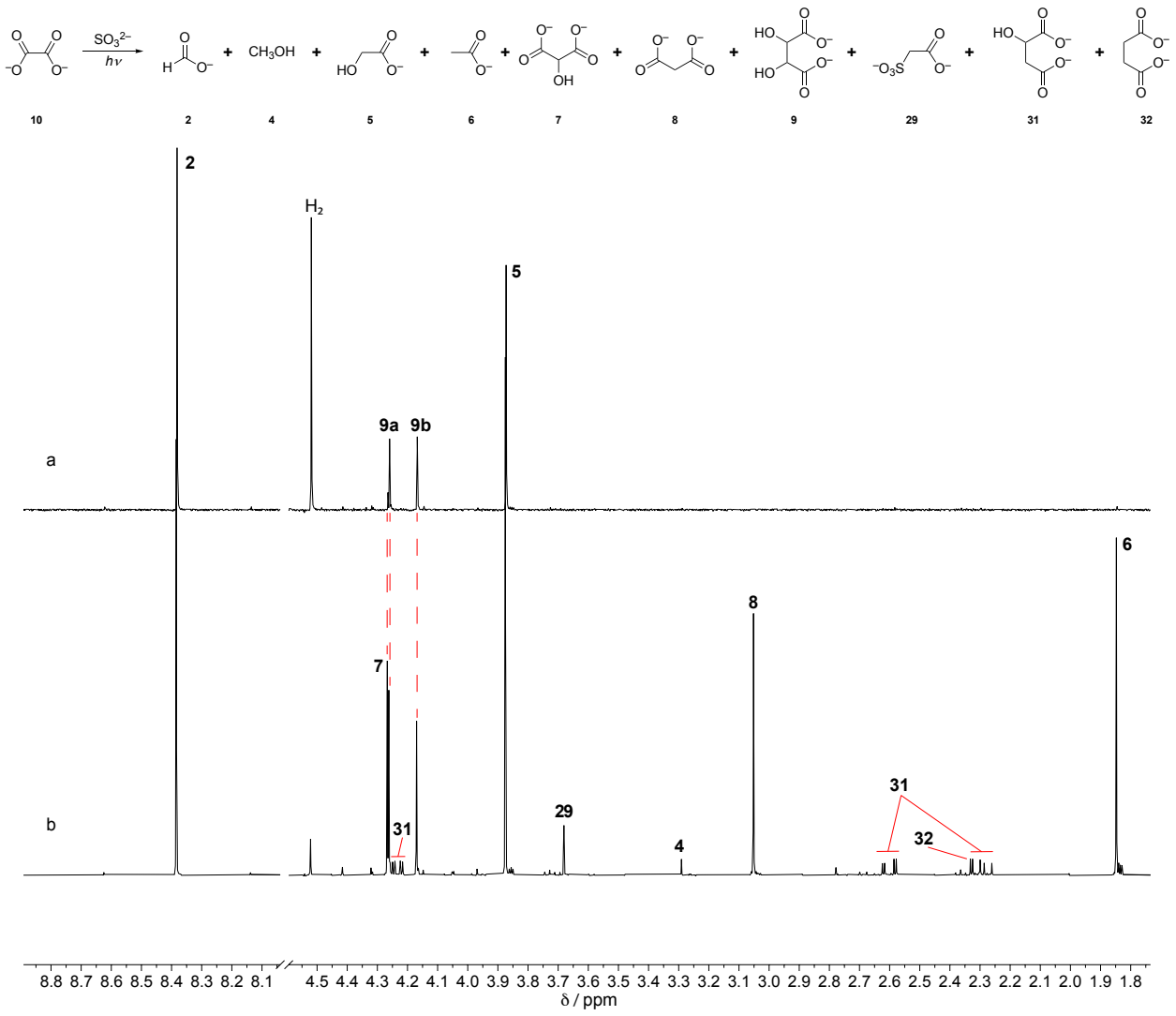

669

670 **Fig. S15.**

671 Stacked ^{1}H-NMR spectra of a solution of sodium oxalate **10** (50 mM) and Na_2SO_3 (100 mM) at
672 pH = 9, a) after 2 hours irradiation; b) after 24 hours irradiation.

673

674

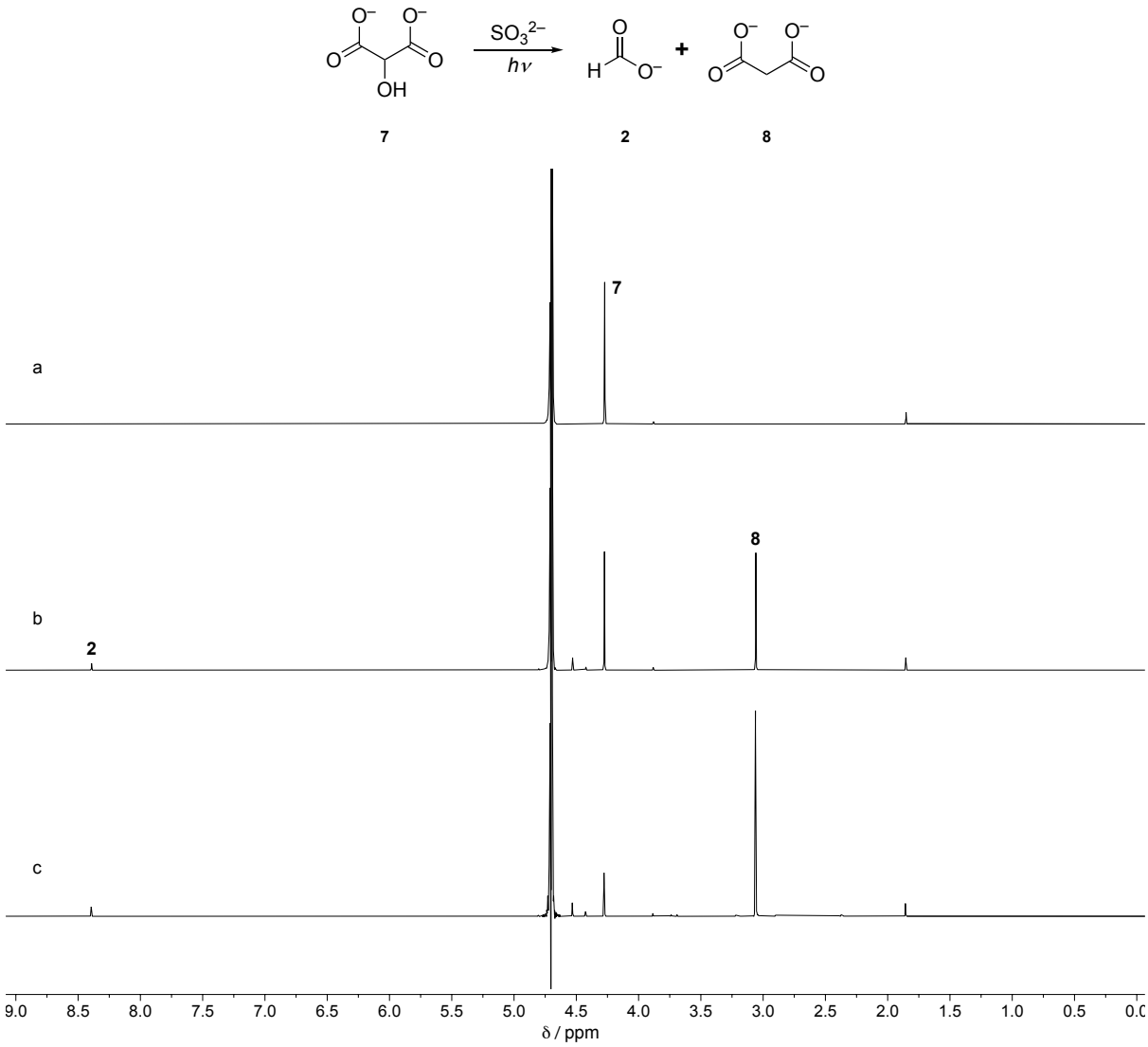

675

676 **Fig. S16.**

677 Stacked ^{1}H-NMR spectra of a solution of sodium tartronate **7** (50 mM) and Na_2SO_3 (100 mM) at
678 pH = 9, a) before irradiation; b) after 2 hours irradiation; c) after 7 hours irradiation.

679

680

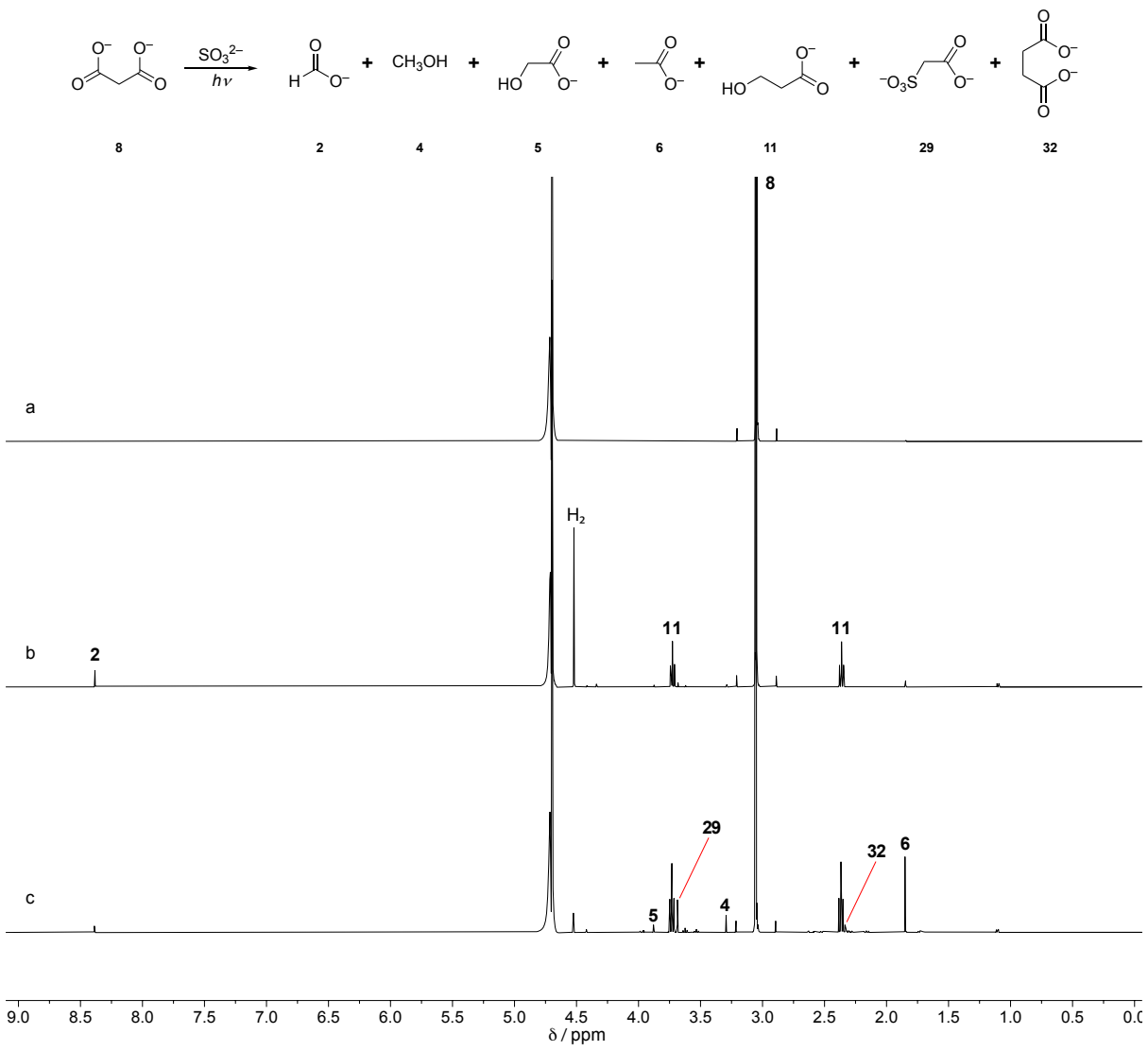

681

682 **Fig. S17.**

683 Stacked ^{1}H-NMR spectra of a solution of sodium malonate **8** (50 mM) and Na_2SO_3 (100 mM) at
684 pH = 9, a) before irradiation; b) after 2 hours irradiation; c) after 20 hours irradiation.
685

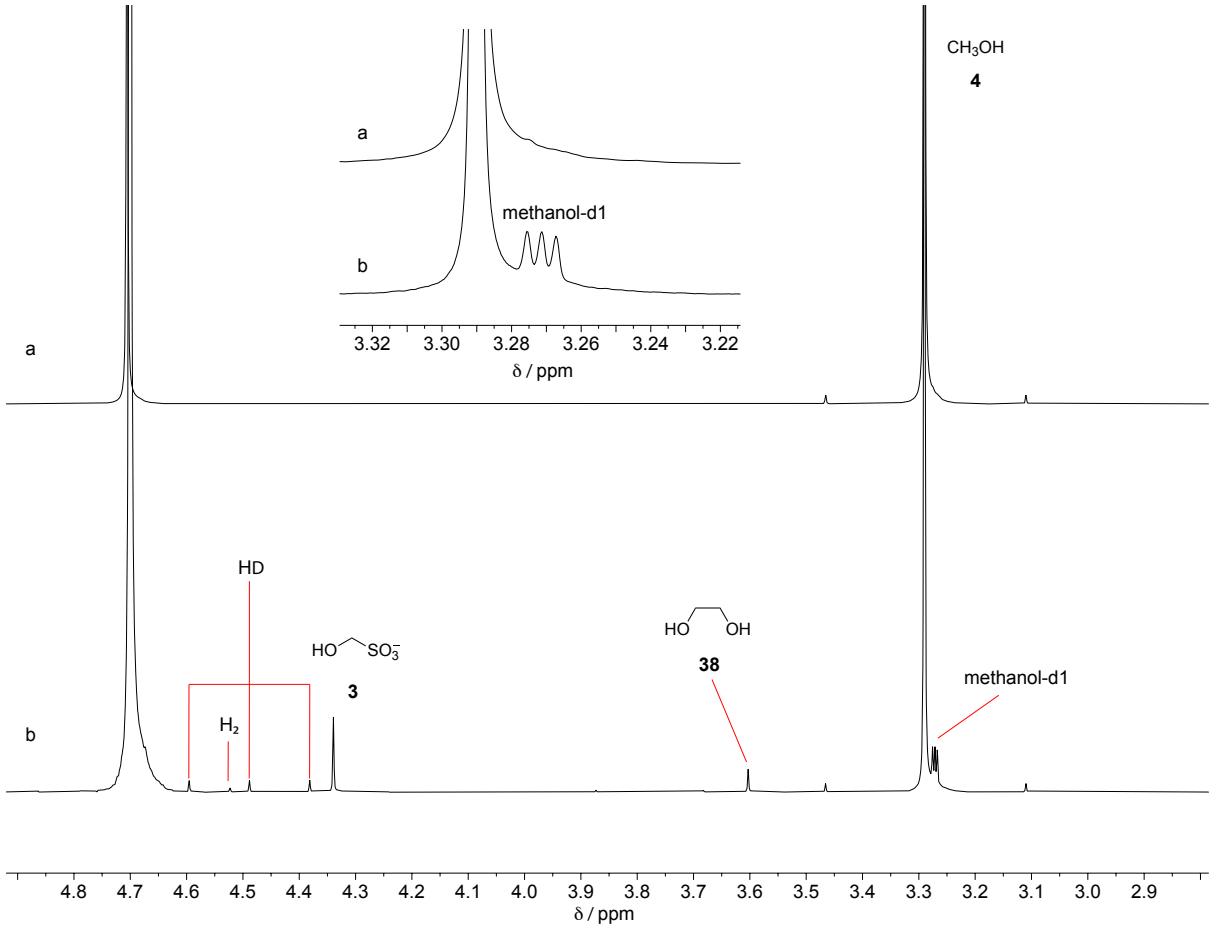

686

687 **Fig. S18.**

688 Stacked ^{1}H-NMR spectra of the reaction of methanol **4** (50 mM), Na_2SO_3 (100 mM) at pD = 9 in
689 99.0 % D_2O, a) before irradiation; b) after 2 hours irradiation. Methanol-d1: CH_2DOH.
690

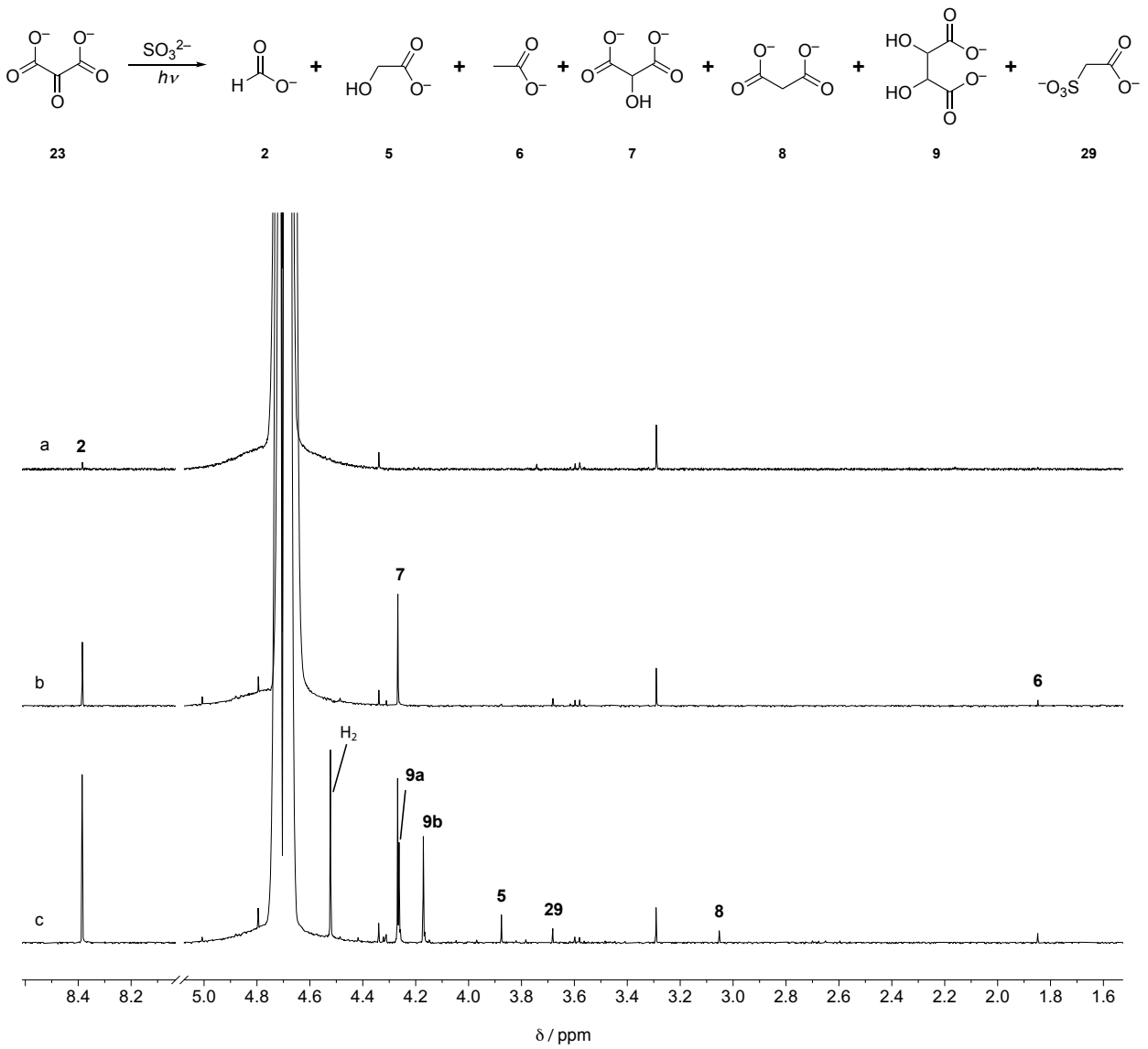

691

692

693 **Fig. S19.**

694 Stacked ^{1}H-NMR spectra of a solution of sodium mesoxalate **23** (50 mM) and Na_2SO_3 (100 mM)
695 at pH = 9, a) before irradiation; b) after 2 hours irradiation; c) after 4 hours irradiation.
696

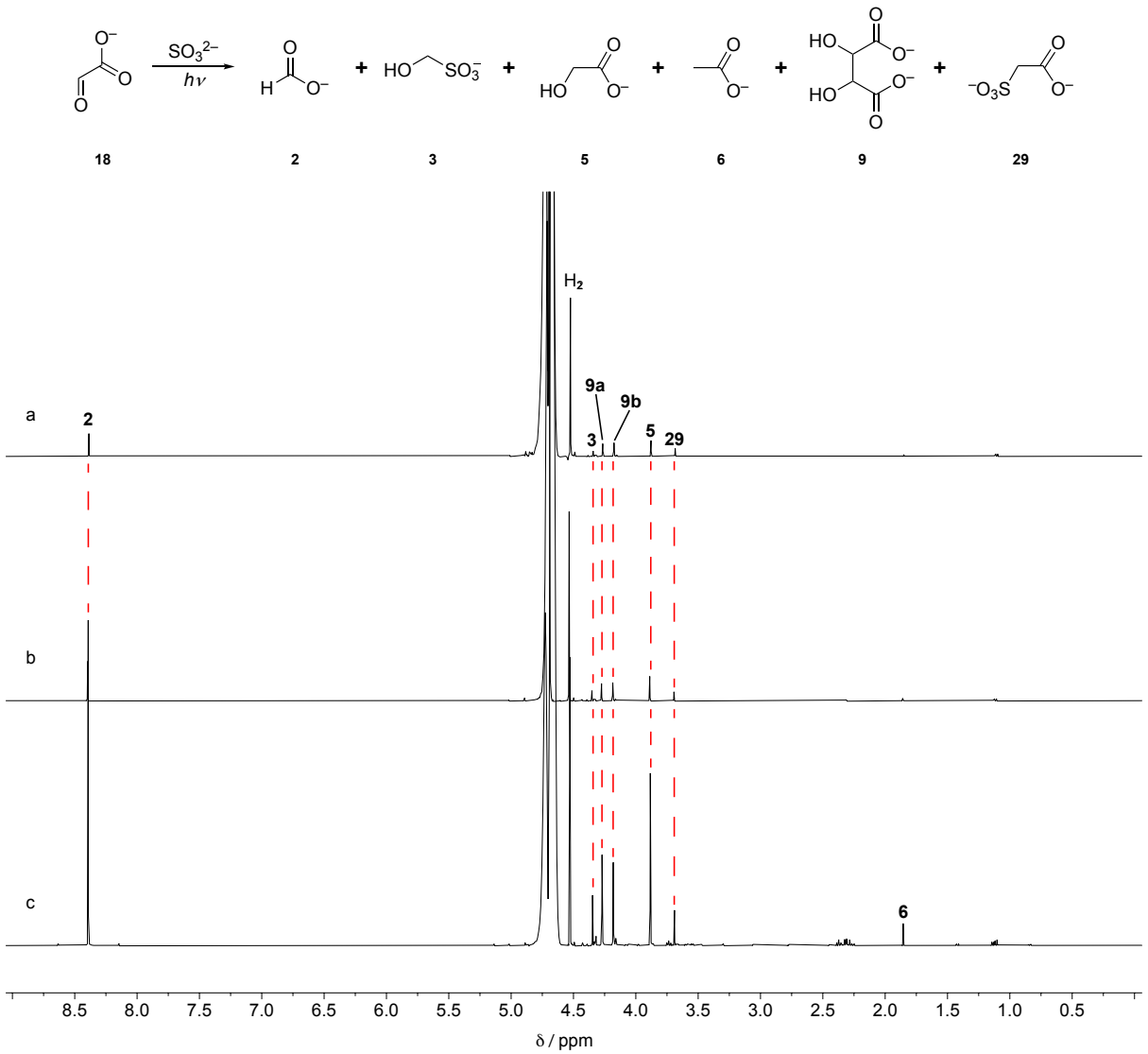

Fig. S20.

Stacked ^{1}H-NMR spectra of a solution of sodium glyoxylate **18** (50 mM) and Na_2SO_3 (100 mM) at pH = 9, a) after 1 hour irradiation; b) after 2 hours irradiation; c) after 6 hours irradiation.

703

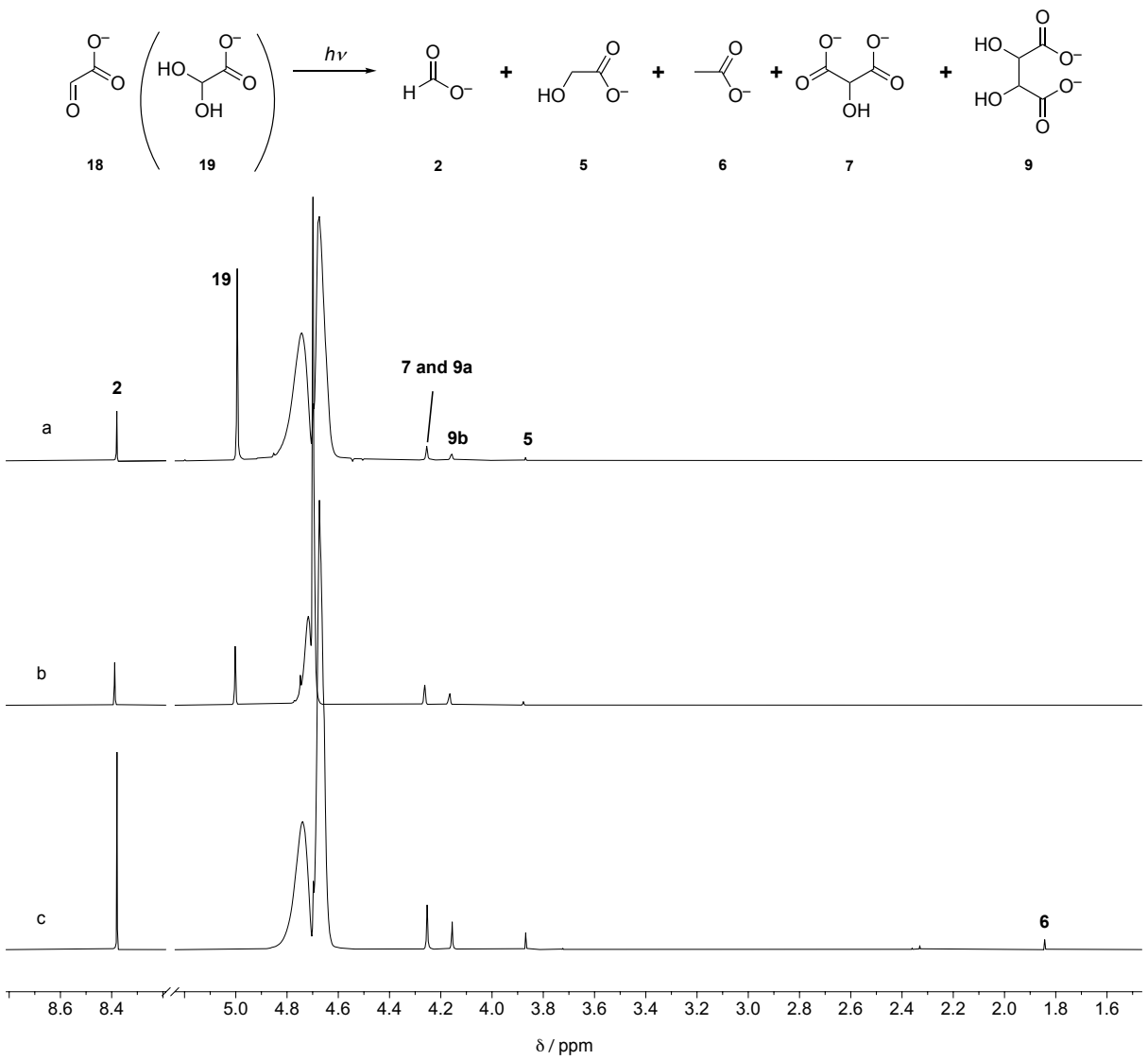

704

705 **Fig. S21.**

706 Stacked ^{1}H-NMR spectra of a solution of sodium glyoxylate **18** (50 mM) at pH = 9, a) after 1
707 hour irradiation; b) after 2 hours irradiation; c) after 6 hours irradiation.
708

709

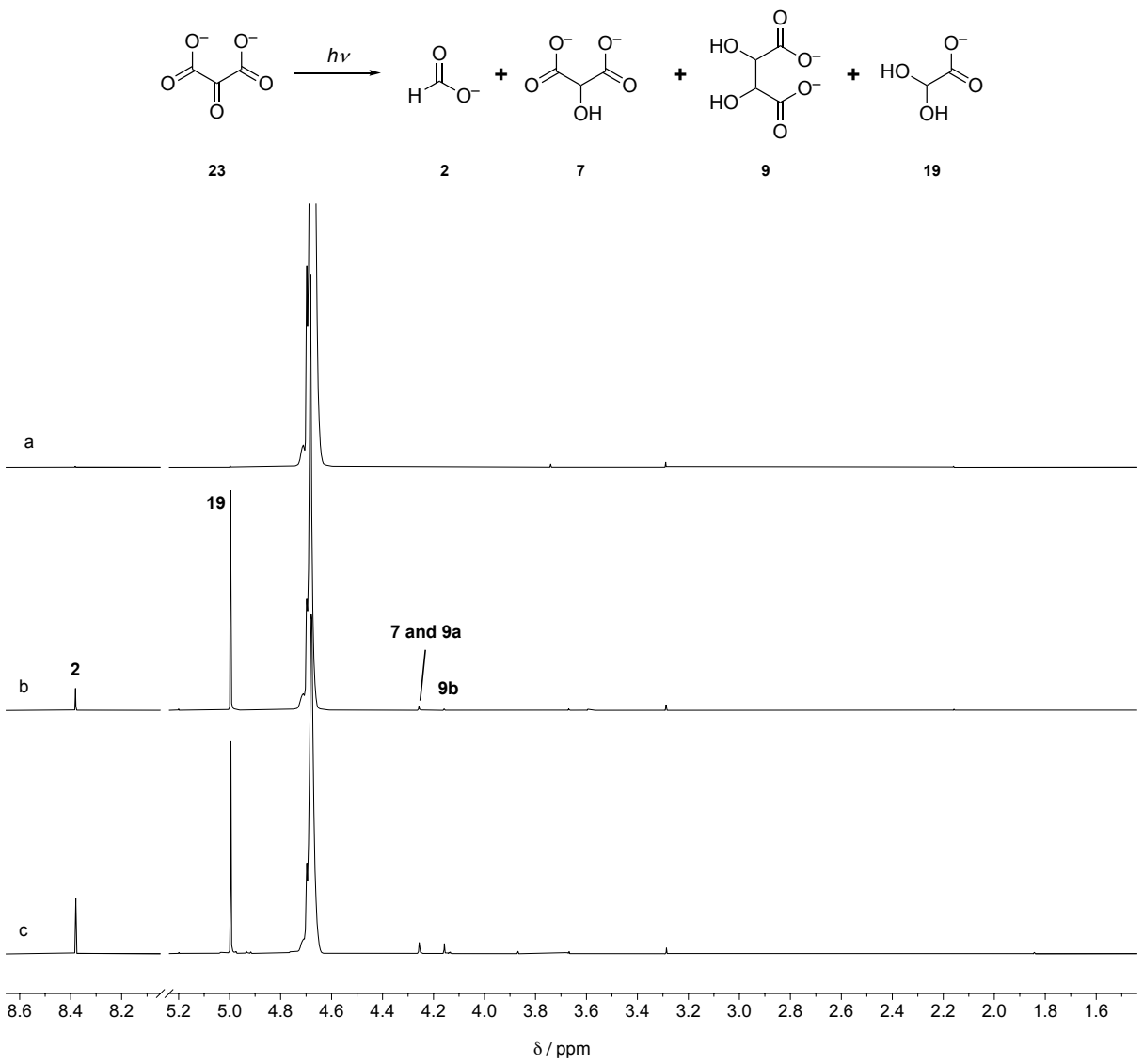

710

711 **Fig. S22.**

712 Stacked ^{1}H-NMR spectra of a solution of sodium mesoxalate **23** (50 mM) at pH = 9, a) before
713 irradiation; b) after 2 hours irradiation; c) after 4 hours irradiation.

714

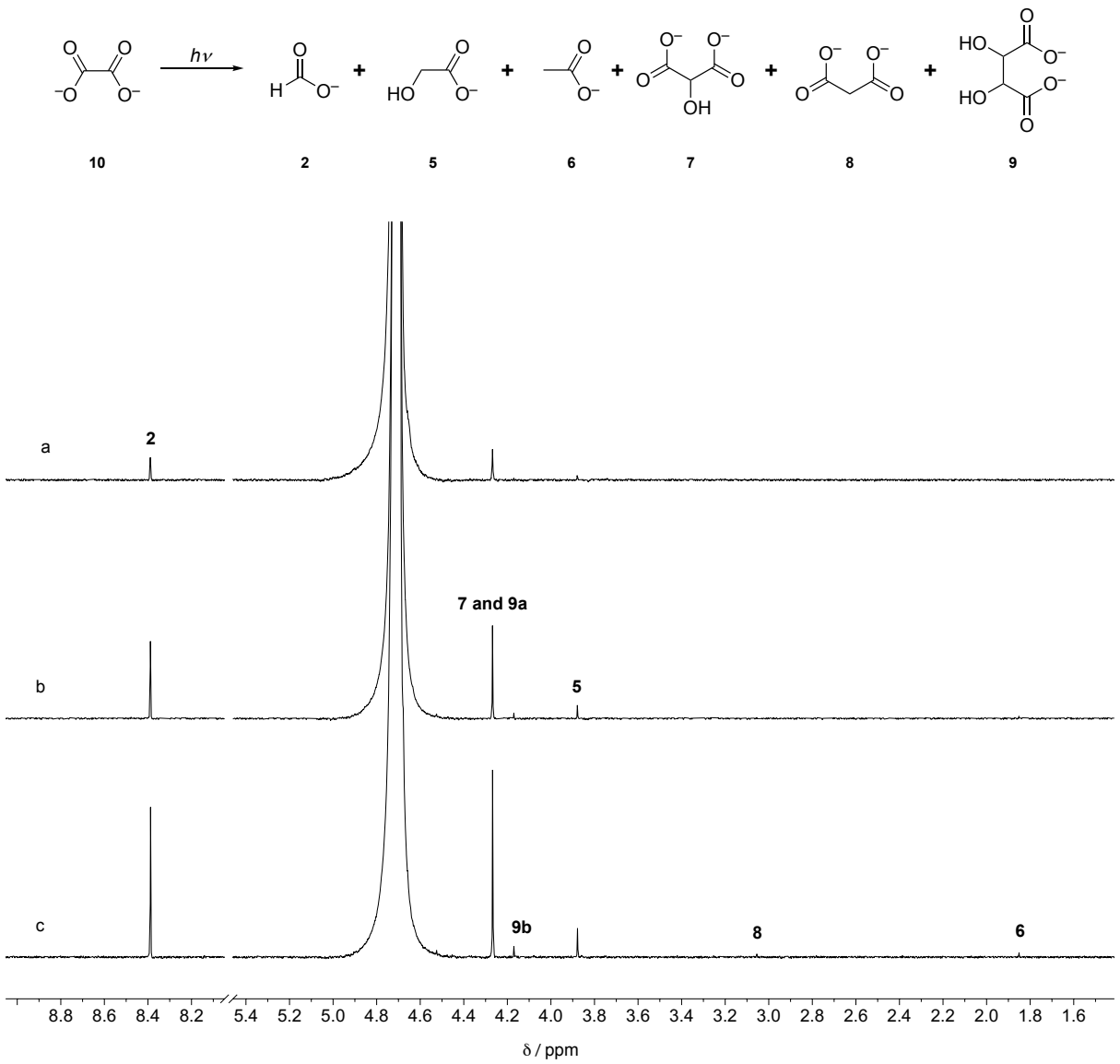

Fig. S23.

Stacked ^{1}H-NMR spectra of a solution of sodium oxalate **10** (50 mM) at pH = 9, a) after 2 hours irradiation; b) after 6 hours irradiation; c) after 10 hours irradiation.

721

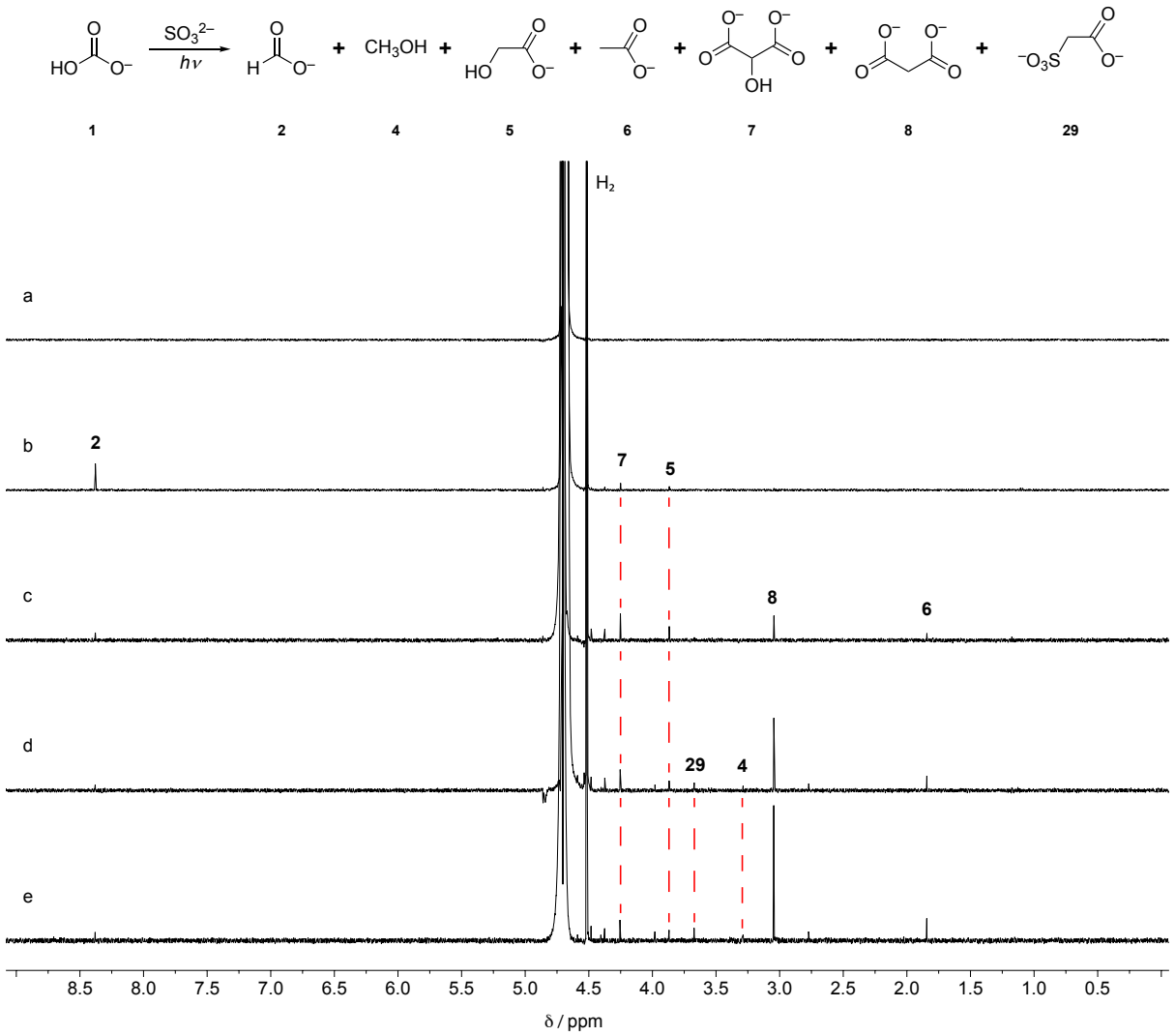

722

723 **Fig. S24.**

724 Stacked ^{1}H-NMR spectra of the reaction of $NaHCO_3$ **1** (5 mM) and Na_2SO_3 (40 mM added
725 portionwise) at pH = 9, a) with Na_2SO_3 (10 mM) before irradiation; b) after irradiation for 1
726 hour; c)-e) after addition of further portions of Na_2SO_3 (each 10 mM) and irradiation for
727 additional 1 hour periods.

728

729

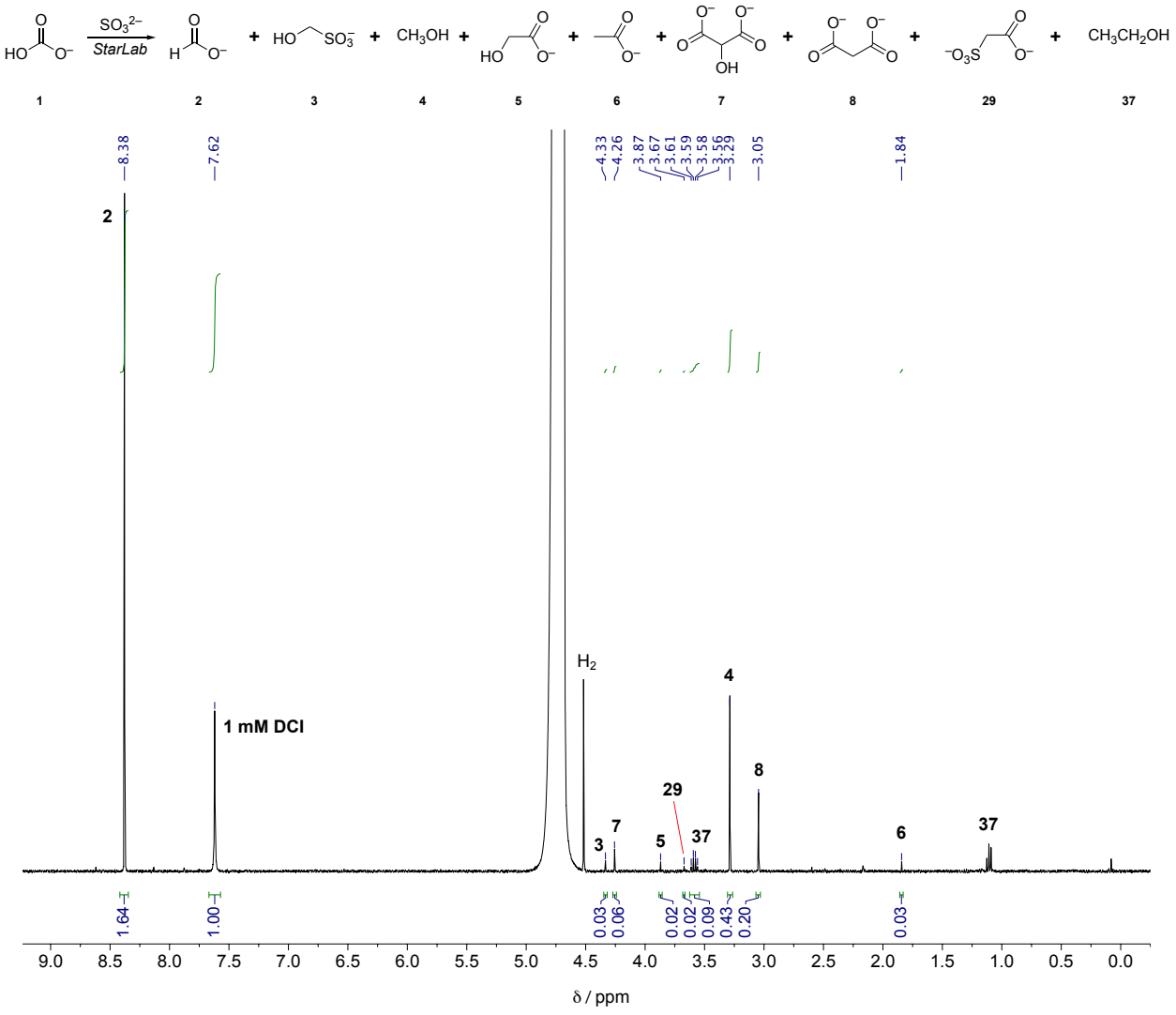

730

731 **Fig. S25.**

732 ^{1}H-NMR spectrum of the reaction products of $NaHCO_3$ **1** (5 mM), Na_2SO_3 (50 mM) at pH = 9
733 after 7 days broadband UV irradiation in the StarLab apparatus, with 4,5-dicyanoimidazole
734 (DCI, 1 mM) added after the reaction as an internal standard.
735

736

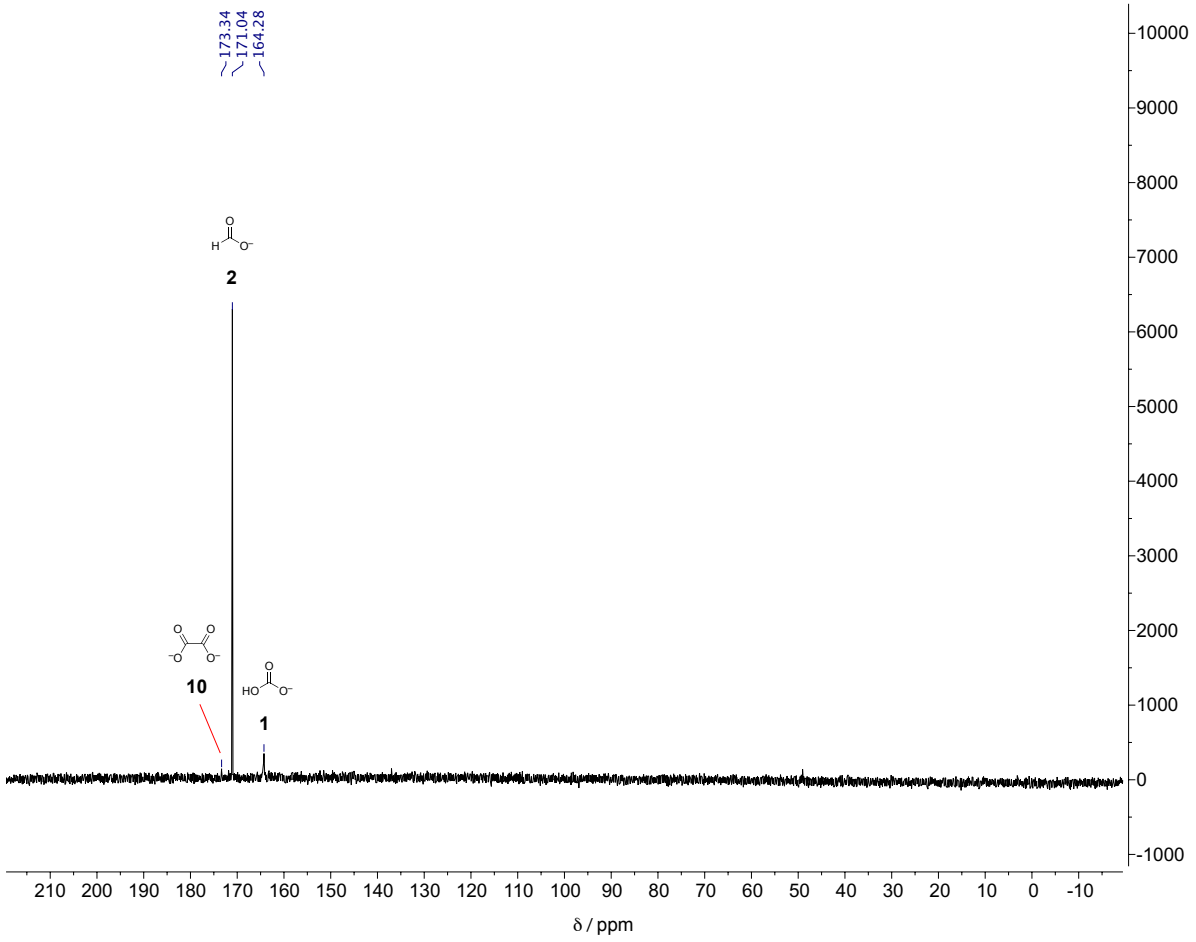

737

738 **Fig. S26.**

739 ^{13}C-NMR spectrum of the reaction products of $NaHCO_3$ **1** (2.5 mM), $NaH^{13}CO_3$ ^{13}C-**1**(2.5 mM),
740 Na_2SO_3 (50 mM) at pH = 9 after 7 days broadband UV irradiation in the StarLab apparatus.

741

742

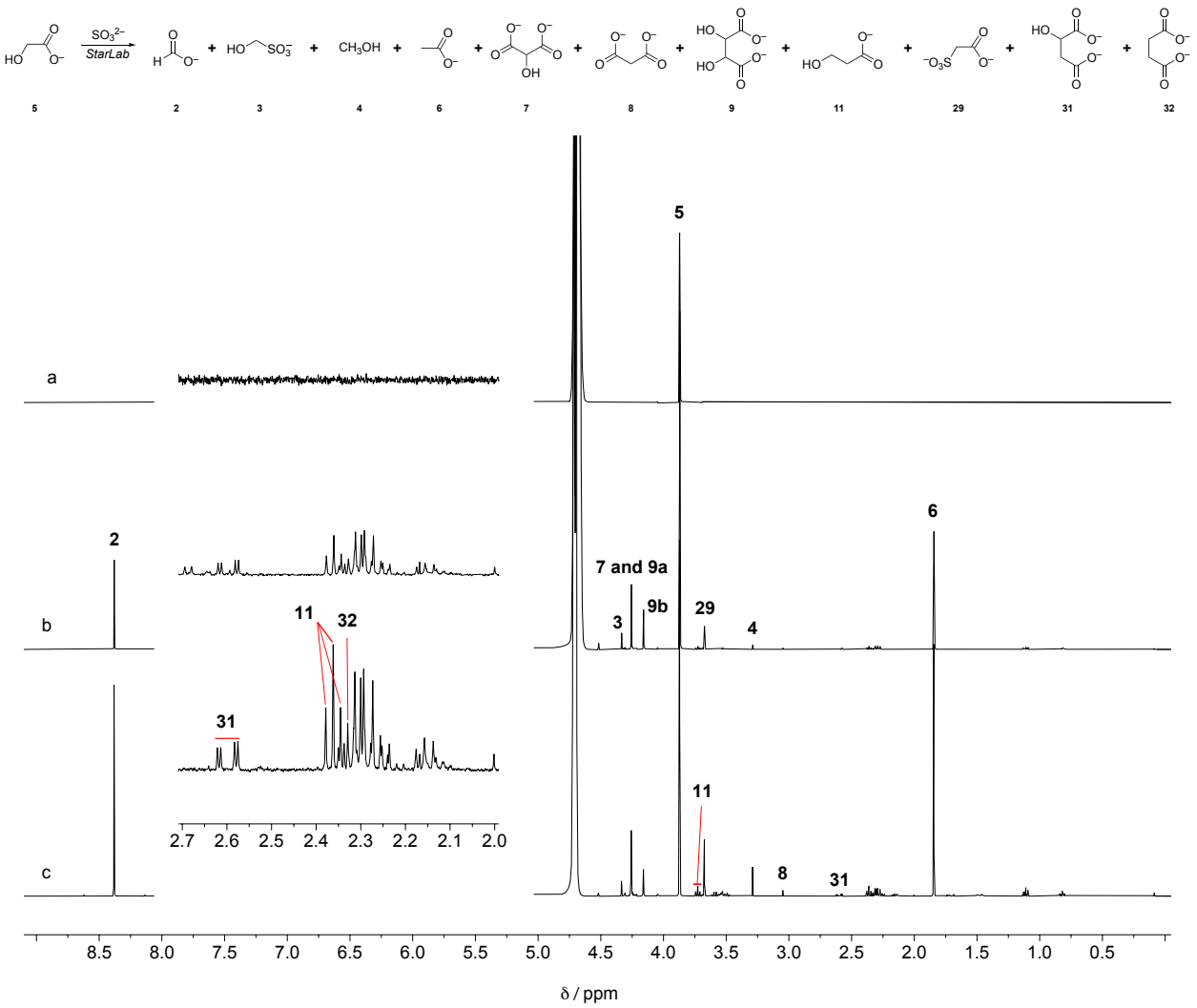

743

744 **Fig. S27.**

745 Stacked ^{1}H-NMR spectra of a solution of sodium glycolate **5** (5 mM), Na_2SO_3 (50 mM) at pH =
746 9, a) before irradiation; b) after 3 days broadband UV irradiation in the StarLab apparatus; c)
747 after 6 days broadband UV irradiation in the StarLab apparatus.

748

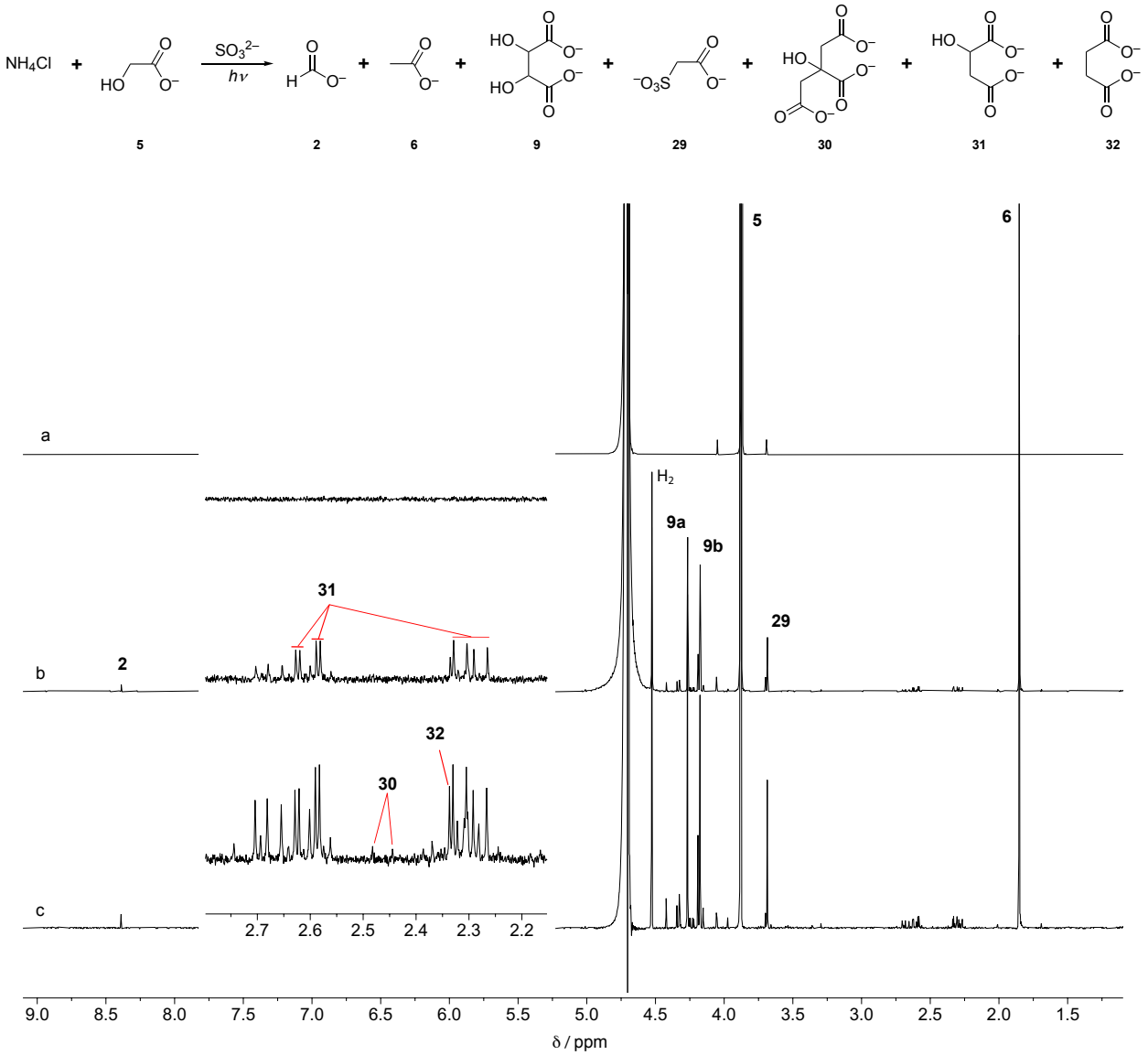

Fig. S28.

Stacked ^{1}H-NMR spectra of a solution of sodium glycolate **5** (50 mM), ammonium chloride (50 mM) and Na_2SO_3 (100 mM) at pH = 9, a) before irradiation; b) after 2 hours irradiation; c) after 4 hours irradiation.

Ultrafast pump-probe spectroscopic investigation of reduction chemistry

The rate constant reported in the literature for reaction of hydrated electrons with formate **2** ($k = 2.4 \times 10^4$ $M^{-1}s^{-1}$)[22] is considerably lower than that for reduction of oxalate (average of three values given in reference[55] is 3.1×10^7 $M^{-1}s^{-1}$). However, in our experiments, oxalate **10** is also prone to photoionization[30-31] and so it was not clear if reaction of hydrated electrons with oxalate in our experiments is, or is not, faster than reaction of hydrated electrons with formate **2**. The rate constant for reaction of hydrated electrons with glycolate **5** ($k = 8.2 \times 10^6$ $M^{-1}s^{-1}$)[28] is high, athough the authors of this paper caution that this "unexpectedly high value may be due to trace impurity in the sample". Furthermore, although the rate constant for reaction of solvated electrons with CO_2 is known[19], we do not know the concentration of CO_2 in our experiments, or whether the catalysis of its interconversion with carbonic acid and bicarbonate by sulfite affects this rate. Accordingly, we used ultrafast pump-probe spectroscopy both to confirm the photoionization of oxalate **10** and compare it to that of sulfite (Fig. S29A), and to measure hydrated electron decay kinetics in mixtures representative of the mixtures used in our continuous irradiation experiments (Table S2). These pump-probe experiments confirmed the photoionization of oxalate **10** and further revealed that bicarbonate, formate **2** and glycolate **5** react at similar rates with hydrated electrons in our experiments, and that oxalate **10** reacts considerably faster (Figure S29 and Tables S1 and S2).

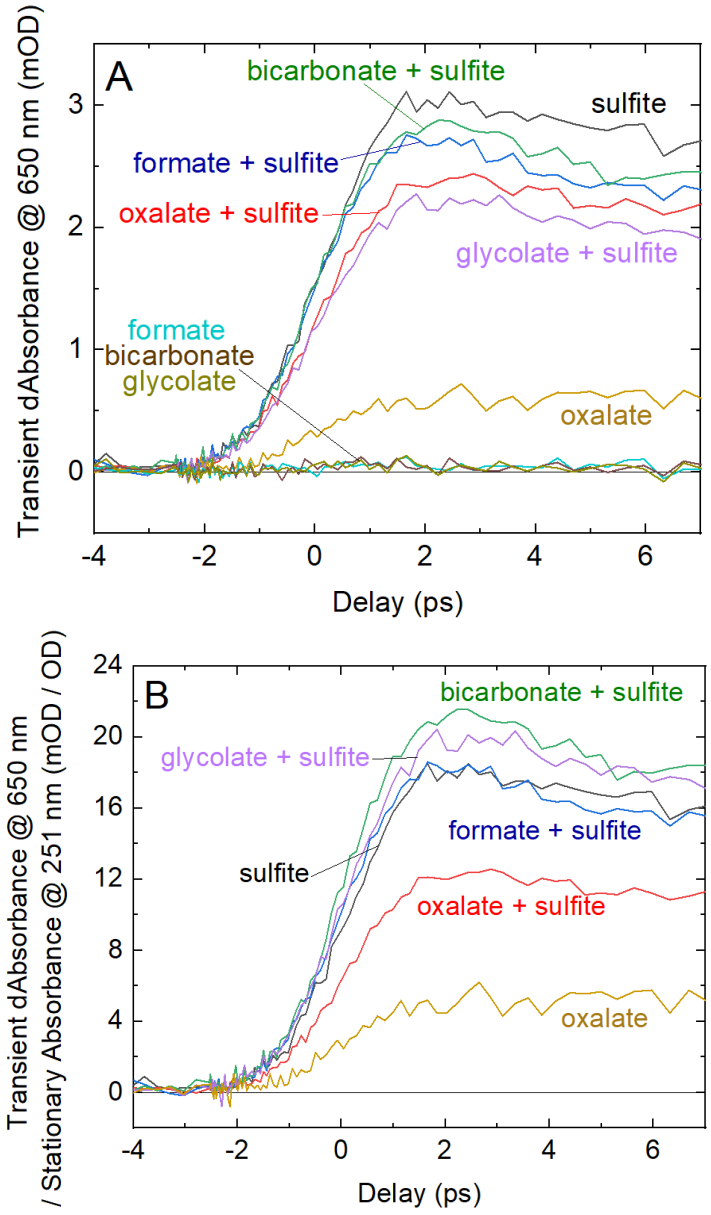

Fig. S29.
Hydrated electron formation induced by UVC (251 nm) irradiation studied by ultrafast pump-probe spectroscopy: (A) Transient absorption signals at 650 nm recorded for different (combinations of) salts in H_2O following 251 nm excitation. The two-photon ionization signal of the solvent has been subtracted and 8 channels adjacent to 650 nm have been averaged. The plot shows the solvent corrected transients up to 7 ps after excitation. (B) Figure A normalized by the stationary UV / Vis sample absorption at 251 nm.

Table. S1. Stationary UV / Vis absorbance at the excitation wavelength (251 nm) and ultrafast (picosecond) absorbance change (dA) maximum probed at 650 nm after 251 nm excitation of different salts (mixtures).

Sample	Absorbance @ 251 nm (OD)	dAbsorbance max. @ 650 nm (mOD)[b]	Concentration of e_{aq} (µM)[c]
sulfite	0.17 ± 0.01	3.0 ± 0.1	19 ± 1
oxalate[a]	0.19 ± 0.01	2.4 ± 0.1	15 ± 1
oxalate	0.12 ± 0.01	0.6 ± 0.1	4 ± 1
glycolate[a]	0.11 ± 0.01	2.2 ± 0.1	14 ± 1
bicarbonate[a]	0.13 ± 0.01	2.8 ± 0.1	18 ± 1
formate[a]	0.15 ± 0.01	2.7 ± 0.1	17 ± 1

a. In the presence of 0.4 M sodium sulfite.
b. Averaged around the maximum between 1.4 ps and 2.9 ps.
c. With the excitation spot (diameter ~300µm, 90:10 level).

The concentrations of UVC-induced hydrated electrons e_{aq} were calculated from the observed dAbsorbance maximum based on Lambert-Beer's law (for homogeneous, non-scattering solutions at low concentration and low light intensities) (I. U. o. P. a. A. Chemistry, *Beer–Lambert law (Beer–Lambert–Bouguer law) Vol. Version 3.0.1*, **2014**.):

$$A(\lambda) = [C] \cdot x \cdot \varepsilon(\lambda) \quad (1)$$

A: Absorbance
λ: Wavelength (here: 650 nm)
[C]: Concentration
x: Sample depth (here: 100 µm)
ε: Molar decadic extinction coefficient, here[56]: ε(650 nm) = 15900 M^{-1} cm^{-1}

$$d[C] = \frac{dA(\lambda)}{x \cdot \varepsilon(\lambda)} \quad (2)$$

Table. S2. Determination of hydrated electron decay lifetimes by ultrafast (microsecond) pump-probe spectroscopy of sulfite alone and in the presence of other carboxylate salts.

Sample	**Salt Concentration [C] (M)**	**Sulfite Concentration (M)**	**Lifetime τ_{el} (s)**	**$[C]^{-1} \cdot \tau_{el}^{-1}$ ($M^{-1} \cdot s^{-1}$)**	**relative $[C]^{-1} \cdot \tau_{el}^{-1}$**
sulfite		0.39 ± 0.03	$(1.7 \pm 0.6) \cdot 10^{-6}$	$(1.5 \pm 0.5) \cdot 10^{6}$	1
oxalate[a]	0.14 ± 0.01	0.24 ± 0.02	$(1.0 \pm 0.3) \cdot 10^{-7}$	$(7 \pm 3) \cdot 10^{7}$	47 ± 16
glycolate[a]	0.24 ± 0.02	0.24 ± 0.02	$(8 \pm 3) \cdot 10^{-7}$	$(5 \pm 2) \cdot 10^{6}$	3.5 ± 1.3
bicarbonate[a]	0.38 ± 0.03	0.37 ± 0.03	$(4.3 \pm 1.5) \cdot 10^{-7}$	$(6 \pm 2) \cdot 10^{6}$	4.0 ± 1.4
formate[a]	0.39 ± 0.03	0.40 ± 0.03	$(8 \pm 3) \cdot 10^{-7}$	$(3.3 \pm 1.2) \cdot 10^{6}$	2.2 ± 0.8

a. In the presence of sodium sulfite.

Reference

55. Buxton, G. V., Greenstock, C. L., Helman, P. & Ross, A. B. Critical Review of rate constants for reactions of hydrated electrons, hydrogen atoms and hydroxyl radicals in aqueous solution. *J. Phys. Chem. Reference Data* **17**, 513–886 (1988).

56. Candeias, L. P., & Steenken, S. Ionization of purine nucleosides and nucleotides and their components by 193-nm laser photolysis in aqueous solution: model studies for oxidative damage of DNA. *J. Am. Chem. Soc.,* **114**, 699-704 (1992).